

February 10, 2016
MITP/16-018

On the precision of a data-driven estimate of hadronic light-by-light scattering in the muon $g - 2$: pseudoscalar-pole contribution

Andreas Nyffeler*

Institut für Kernphysik and PRISMA Cluster of Excellence,
Johannes Gutenberg-Universität Mainz, D-55128 Mainz, Germany

Abstract

The evaluation of the numerically dominant pseudoscalar-pole contribution to hadronic light-by-light scattering in the muon $g - 2$ involves the pseudoscalar-photon transition form factor $\mathcal{F}_{P\gamma^*\gamma^*}(-Q_1^2, -Q_2^2)$ with $P = \pi^0, \eta, \eta'$ and, in general, two off-shell photons with spacelike momenta $Q_{1,2}^2$. We show, in a largely model-independent way, that for π^0 (η, η') the region of photon momenta below about 1 (1.5) GeV gives the main contribution to hadronic light-by-light scattering. We then discuss how the precision of current and future measurements of the single- and double-virtual transition form factor in different momentum regions impacts the precision of a data-driven estimate of this contribution to hadronic light-by-light scattering. Based on Monte Carlo simulations for a planned first measurement of the double-virtual form factor at BESIII, we find that for the π^0, η, η' -pole contributions a precision of 14%, 23%, 15% seems feasible. Further improvements can be expected from other experimental data and also from the use of dispersion relations for the different form factors themselves.

*nyffeler@kph.uni-mainz.de

1 Introduction

The anomalous magnetic moment of the muon $a_\mu = (g - 2)/2$ has served for many years as important test of the Standard Model (SM) of particle physics, see Refs. [1, 2, 3, 4] which review theory and experiment and contain many references to earlier work. The contributions from the different sectors in the SM and the current experimental value, largely dominated by the measurement at Brookhaven [5], corrected for a small shift in the ratio of the magnetic moments of the muon and the proton [6], have been collected in Table 1. For the muon $g - 2$, all sectors of the SM contribute significantly at the current level of precision. The QED contribution dominates numerically, but it is very precisely known up to 5-loop order [7]. Also the electroweak contribution is under control at the two-loop level, including a small hadronic uncertainty and estimates of leading three-loop contributions [8]. The main source of uncertainty originates from the hadronic contributions from vacuum polarization (HVP) and light-by-light scattering (HLbL) at various orders in the electromagnetic coupling α . Comparing SM theory and experiment, a discrepancy of 3 – 5 standard deviations is observed for several years now.¹ This deviation could be a sign of New Physics beyond the SM [1, 2, 3, 4], but the large hadronic uncertainties make it difficult to draw firm conclusions. These uncertainties need to be reduced and better controlled [15], also in view of planned future muon $g - 2$ experiments at Fermilab and J-PARC which will try to reduce the experimental error by a factor of four to about $\delta a_\mu^{\text{exp}} = 16 \times 10^{-11}$ [16].

Table 1: Contributions to the muon $g - 2$ from the different sectors in the SM and comparison of theory and experiment.

Contribution	$a_\mu \times 10^{11}$	Reference
QED (leptons + photons)	116 584 718.853 \pm 0.036	[7]
Electroweak	153.6 \pm 1.0	[8]
HVP: LO	6907.5 \pm 47.2	[9]
NLO	-100.3 \pm 2.2	[9]
NNLO	12.4 \pm 0.1	[10]
HLbL	116 \pm 40	[11, 2]
NLO	3 \pm 2	[12]
Theory (SM)	116 591 811 \pm 62	—
Experiment	116 592 089 \pm 63	[5, 6]
Experiment - Theory (3.1 σ)	278 \pm 88	—

¹The absolute and relative size of the deviation depends on the treatment of the hadronic contributions and how aggressively the errors are estimated. See Ref. [13] for other recent evaluations of the HVP contribution.

While the HVP contribution can be improved systematically with measurements of the cross section $\sigma(e^+e^- \rightarrow \text{hadrons})$, the often used estimates for HLbL

$$a_\mu^{\text{HLbL}} = (105 \pm 26) \times 10^{-11}, \quad [17] \quad (1)$$

$$a_\mu^{\text{HLbL}} = (116 \pm 40) \times 10^{-11}, \quad [11, 2] \quad (2)$$

are both largely based on the same model calculations [18, 19, 20, 21, 22], which suffer from partly uncontrollable uncertainties. Therefore the error estimates in Eqs. (1) and (2) are essentially just guesses. Note that the central values probably need to be shifted downwards to $a_\mu^{\text{HLbL}} = (98 \pm 26) \times 10^{-11}$ for [17] and $a_\mu^{\text{HLbL}} = (102 \pm 40) \times 10^{-11}$ for [11, 2], since recent reevaluations [23, 24, 14] of the axial-vector contribution yield a smaller value $a_\mu^{\text{HLbL;axial}} = (8 \pm 3) \times 10^{-11}$ compared to the result $a_\mu^{\text{HLbL;axial}} = (22 \pm 5) \times 10^{-11}$ obtained in Ref. [22] and used in Refs. [11, 2]. Ref. [17] had already used a somewhat smaller value $a_\mu^{\text{HLbL;axial}} = (15 \pm 10) \times 10^{-11}$. Furthermore, after the publication of Refs. [17, 11, 2], there were claims in Refs. [25, 26] using different models that the dressed quark-loop contribution might be around 110×10^{-11} , i.e. much bigger than for instance the value $(21 \pm 3) \times 10^{-11}$ estimated in Ref. [20]. Moreover, in Ref. [27] it was argued that also the pion-loop contribution could be potentially bigger in absolute size, $-(11 - 71) \times 10^{-11}$, compared to $-(19 \pm 13) \times 10^{-11}$ in Ref. [20]. See Ref. [28] for an analysis of these claims and a brief review on other recent developments in HLbL.

There are attempts ongoing to calculate the HLbL contribution to the muon $g - 2$ from first principles in Lattice QCD. A first, still incomplete, result was obtained recently in Ref. [29] which contains references to earlier work in the last years. Another approach was proposed in Ref. [30]. It remains to be seen, how fast reliable estimates for HLbL can be obtained within Lattice QCD, where all systematic uncertainties of the extrapolations to physical quark masses (physical pion masses), to the continuum and to infinite volume are fully under control and also all quark-disconnected contributions are included.

In this situation, a dispersive approach to HLbL was proposed recently in Refs. [31, 32], which tries, in the spirit of the HVP calculation, to relate the presumably numerically dominant contributions from the pseudoscalar-*poles* and the pion-loop with *on-shell* intermediate pseudoscalar states to, in principle, measurable form factors and cross-sections with off-shell photons:

$$\gamma^* \gamma^* \rightarrow \pi^0, \eta, \eta', \quad (3)$$

$$\gamma^* \gamma^* \rightarrow \pi^+ \pi^-, \pi^0 \pi^0. \quad (4)$$

The two dispersive approaches differ somewhat. Ref. [31] considers first the four-point function $\langle VVVV \rangle$ with three off-shell and one on-shell photons, then identifies the intermediate on-shell hadronic states and then projects on the muon $g - 2$. On the other hand, Ref. [32] writes down directly a dispersion relation for the Pauli form factor $F_2(k^2)$ and evaluates the imaginary part of $F_2(k^2)$ from the various multi-particle cuts with hadrons and photons in the Feynman diagrams, and then calculates $a_\mu = F_2(0)$.

The hope is that this data-driven estimate for HLbL will allow a 10% precision for these contributions, with a reliable and controllable error related to the experimental

measurement precision, and that the remaining, hopefully smaller contributions, e.g. from axial-vectors (3π -intermediate state), other heavier states and a dressed quark-loop, properly matched to perturbative QCD and avoiding double-counting, can be obtained within models with about 30% uncertainty to reach an overall, reliable precision goal of about 20% ($\delta a_\mu^{\text{HLbL}} \approx 20 \times 10^{-11}$).

In this paper we will concentrate on the dispersive approach to the pseudoscalar-pole contribution to HLbL which is numerically dominant according to most model calculations. It arises from the one-particle intermediate states of the light pseudoscalars π^0, η, η' shown in the Feynman diagrams in Fig. 1. The blobs in the Feynman diagrams represent

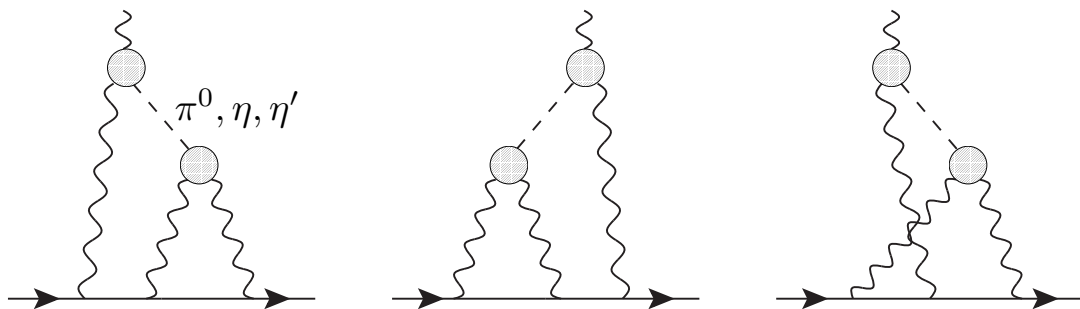


Figure 1: The pseudoscalar-pole contribution to hadronic light-by-light scattering. The shaded blobs represent the transition form factor $\mathcal{F}_{P\gamma^*\gamma^*}(q_1^2, q_2^2)$ where $P = \pi^0, \eta, \eta'$.

the double-virtual transition form factor $\mathcal{F}_{P\gamma^*\gamma^*}(q_1^2, q_2^2)$ where $P = \pi^0, \eta, \eta'$. See Ref. [33] for a recent brief overview on transition form factors (TFF), many more details can be found in the older review [34].²

In order to simplify the notation, we will now discuss mainly the neutral pion-pole contribution. The generalization to the pole contributions of η and η' is straightforward. The pion-photon transition form factor $\mathcal{F}_{\pi^0\gamma^*\gamma^*}(q_1^2, q_2^2)$ is defined by the following vertex function in QCD:

$$i \int d^4x e^{iq_1 \cdot x} \langle 0 | T \{ j_\mu(x) j_\nu(0) \} | \pi^0(q_1 + q_2) \rangle = \varepsilon_{\mu\nu\alpha\beta} q_1^\alpha q_2^\beta \mathcal{F}_{\pi^0\gamma^*\gamma^*}(q_1^2, q_2^2). \quad (5)$$

Here $j_\mu(x) = (\bar{\psi} \hat{Q} \gamma_\mu \psi)(x)$ is the light quark part of the electromagnetic current ($\bar{\psi} \equiv (\bar{u}, \bar{d}, \bar{s})$ and $\hat{Q} = \text{diag}(2, -1, -1)/3$ is the charge matrix). The form factor describes the interaction of an on-shell neutral pion with two off-shell photons with four-momenta q_1 and q_2 . It is Bose symmetric, $\mathcal{F}_{\pi^0\gamma^*\gamma^*}(q_1^2, q_2^2) = \mathcal{F}_{\pi^0\gamma^*\gamma^*}(q_2^2, q_1^2)$, because the two photons

²More generally, one can define a pseudoscalar-*exchange* contribution to HLbL which involves a form factor with off-shell pseudoscalars $\mathcal{F}_{P^*\gamma^*\gamma^*}((q_1 + q_2)^2, q_1^2, q_2^2)$ [18, 20, 35, 11, 2], but then the contribution to HLbL is model-dependent. In particular, it will depend on the interpolating field used for the pseudoscalars.

are indistinguishable. The form factor for real photons is related to the decay width into two photons: $\mathcal{F}_{\pi^0\gamma^*\gamma^*}^2(0,0) = 4\Gamma(\pi^0 \rightarrow \gamma\gamma)/(\pi\alpha^2 m_\pi^3)$. Often the normalization with the chiral anomaly is used $\mathcal{F}_{\pi^0\gamma^*\gamma^*}(0,0) = -N_c/(12\pi^2 F_\pi)$.

If one evaluates only the pion-pole contribution of the Feynman diagrams and projects on the muon $g-2$, one obtains the result [21]

$$a_\mu^{\text{HLbL};\pi^0} = \left(\frac{\alpha}{\pi}\right)^3 \left[a_\mu^{\text{HLbL};\pi^0(1)} + a_\mu^{\text{HLbL};\pi^0(2)} \right], \quad (6)$$

$$a_\mu^{\text{HLbL};\pi^0(1)} = \int \frac{d^4 q_1}{(2\pi)^4} \frac{d^4 q_2}{(2\pi)^4} \frac{1}{q_1^2 q_2^2 (q_1 + q_2)^2 [(p + q_1)^2 - m_\mu^2] [(p - q_2)^2 - m_\mu^2]} \\ \times \frac{\mathcal{F}_{\pi^0\gamma^*\gamma^*}(q_1^2, (q_1 + q_2)^2) \mathcal{F}_{\pi^0\gamma^*\gamma^*}(q_2^2, 0)}{q_2^2 - m_\pi^2} \tilde{T}_1(q_1, q_2; p), \quad (7)$$

$$a_\mu^{\text{HLbL};\pi^0(2)} = \int \frac{d^4 q_1}{(2\pi)^4} \frac{d^4 q_2}{(2\pi)^4} \frac{1}{q_1^2 q_2^2 (q_1 + q_2)^2 [(p + q_1)^2 - m_\mu^2] [(p - q_2)^2 - m_\mu^2]} \\ \times \frac{\mathcal{F}_{\pi^0\gamma^*\gamma^*}(q_1^2, q_2^2) \mathcal{F}_{\pi^0\gamma^*\gamma^*}((q_1 + q_2)^2, 0)}{(q_1 + q_2)^2 - m_\pi^2} \tilde{T}_2(q_1, q_2; p), \quad (8)$$

where $p^2 = m_\mu^2$ (on-shell muon) and the external photon has now zero four-momentum (soft photon). The kinematic functions $\tilde{T}_{1,2}(q_1, q_2; p)$ are reproduced in Appendix A. The first and the second graphs in Fig. 1 give rise to identical contributions, leading to the term with \tilde{T}_1 . The third graph yields the contribution involving \tilde{T}_2 .

There have been objections [36] raised recently about the implementation of the dispersive approach for the pion-pole contribution in Refs. [31, 32]. According to the arguments in Refs. [22, 36] there should be no form factor at the external vertex with the soft-photon. This amounts to setting the single-virtual form factors $\mathcal{F}_{\pi^0\gamma^*\gamma^*}(q^2, 0)$ in Eqs. (7) and (8) to a constant. Maybe the disagreement arises whether one interprets the diagrams in Fig. 1 as genuine Feynman diagrams contributing to the muon $g-2$ or as unitarity diagrams often used in the context of dispersive approaches. In Ref. [32] it was shown, however, that when one writes down a dispersion relation for the Pauli form factor $F_2(k^2)$ and evaluates the imaginary part of $F_2(k^2)$ from the various two-particle and three-particle cuts in the Feynman diagrams, and then calculates $a_\mu = F_2(0)$, one obtains for a simple Vector Meson Dominance (VMD) model for the form factor exactly the expressions in Eqs. (7) and (8) *with* a form factor at the external vertex. We will therefore use the prescription from Refs. [21, 31, 32] to study the pseudoscalar-pole contribution $a_\mu^{\text{HLbL};P}$ to HLbL.

Most model evaluations of $a_\mu^{\text{HLbL};\pi^0}$ (pion-pole defined in different ways or pion-exchange with off-shell-pion form factors) and $a_\mu^{\text{HLbL};P}$, with $P = \pi^0, \eta, \eta'$, agree at the level of 15%, but the full range of estimates (central values) is much larger [37]:

$$a_{\mu;\text{models}}^{\text{HLbL};\pi^0} = (50 - 80) \times 10^{-11} = (65 \pm 15) \times 10^{-11} \quad (\pm 23\%), \quad (9)$$

$$a_{\mu;\text{models}}^{\text{HLbL};P} = (59 - 114) \times 10^{-11} = (87 \pm 27) \times 10^{-11} \quad (\pm 31\%). \quad (10)$$

This situation has to be improved without relying too much on various models, in particular before the new muon $g-2$ experiment at Fermilab yields results with a four-fold improvement over the Brookhaven experiment in a few years [16]. In this paper we

therefore study, as model-independently as possible, which are the most important momentum regions for the pseudoscalar-pole contribution $a_\mu^{\text{HLbL;P}}$. We also analyze what is the impact of the precision of current and future measurements of the single-virtual $\mathcal{F}_{\text{P}\gamma^*\gamma^*}(q^2, 0)$ and the double-virtual pseudoscalar transition form factor $\mathcal{F}_{\text{P}\gamma^*\gamma^*}(q_1^2, q_2^2)$ in different momentum regions on the uncertainty of a data-driven estimate of this contribution to HLbL. We hope that this information will be a valuable guide to help the experimental community to plan, design and analyze the measurements of decay rates, form factors and cross-sections of the light pseudoscalars π^0, η, η' and their interactions with off-shell photons. In a way, our approach is a generalization of the pie-charts often shown for the HVP contribution and its error as a function of the center-of-mass energy \sqrt{s} in $\sigma(e^+e^- \rightarrow \text{hadrons})$ [2]. However, since HLbL involves different amplitudes [20, 31, 41] which depend on several invariant momenta, the situation is of course more complicated than for the HVP contribution.

This paper is organized as follow. Section 2 recalls the three-dimensional integral representation for the pseudoscalar-pole contribution $a_\mu^{\text{HLbL;P}}$ derived in Ref. [2] which separates model-independent weight functions $w_{1,2}(Q_1, Q_2, \cos\theta)$ from the dependence on the form factor $\mathcal{F}_{\text{P}\gamma^*\gamma^*}(-Q_1^2, -Q_2^2)$ for spacelike (Euclidean) momenta with magnitude $Q_{1,2}$ and angle θ between the momentum vectors. In Section 3 the weight functions for π^0, η and η' are analyzed in detail. Several three-dimensional plots (as function of the two momenta $Q_{1,2}$) and one-dimensional plots (as function of the angle θ) are shown and the maxima and minima of the weight functions are determined. The relevant momentum regions for $a_\mu^{\text{HLbL;P}}$ in different bins in the (Q_1, Q_2) -plane are identified in Section 4 within two simple models for the TFF, since the loop integral in Eq. (7) diverges without a form factor which dampens the large momentum region. Section 5 summarizes the experimental status on the precision of measurements of the TFF for π^0, η and η' . This is based on data for the two-photon decay width $\Gamma(\text{P} \rightarrow \gamma\gamma)$, the slope of the form factor at zero momentum and data for the single-virtual form factor $\mathcal{F}_{\text{P}\gamma^*\gamma^*}(-Q^2, 0)$ in the spacelike and timelike momentum region. For the double-virtual form factor $\mathcal{F}_{\text{P}\gamma^*\gamma^*}(-Q_1^2, -Q_2^2)$ there is currently no experimental data available. We use the results of a Monte Carlo (MC) simulation [42] for planned measurements of this form factor at the BESIII detector to estimate the potential precision which could be reached in the next few years. Section 6 then discusses the impact of the experimental uncertainties for the TFF on $a_\mu^{\text{HLbL;P}}$ and points out in which specific momentum regions (momentum bins) a high experimental precision of TFF is needed for a precise data-driven estimate of the pseudoscalar-pole contribution to HLbL. Finally, Section 7 presents a summary of our findings and the conclusions. In Appendix A we reproduce the formulae for the kinematic functions $\tilde{T}_{1,2}$ in the loop-integrals in Eqs. (7) and (8) from Ref. [21] and the weight functions $w_{1,2}$ from Ref. [2]. We give the Taylor expansions for the weight functions in various limits (small and large momenta, collinear momenta). A brief summary of the two form factor models that we use in our numerical analysis can be found in Appendix B.

2 Three-dimensional integral representation for the pseudoscalar-pole contribution $a_\mu^{\text{HLbL};\text{P}}$

We concentrate again mainly on the pion-pole contribution in this Section. After a Wick rotation to Euclidean momenta $Q_i, i = 1, 2$, and averaging over the direction of the muon momentum p using the method of Gegenbauer polynomials (hyperspherical approach) [43], one can perform for arbitrary form factors in the two-loop integrals (7) and (8) all angular integrations, except one over the angle θ between the four-momenta Q_1 and Q_2 which also appears through $Q_1 \cdot Q_2$ in the form factors. In this way one obtains the following three-dimensional integral representation for the pion-pole contribution with on-shell-pion transition form factors [2]

$$a_\mu^{\text{HLbL};\pi^0(1)} = \int_0^\infty dQ_1 \int_0^\infty dQ_2 \int_{-1}^1 d\tau w_1(Q_1, Q_2, \tau) \times \mathcal{F}_{\pi^0\gamma^*\gamma^*}(-Q_1^2, -(Q_1 + Q_2)^2) \mathcal{F}_{\pi^0\gamma^*\gamma^*}(-Q_2^2, 0), \quad (11)$$

$$a_\mu^{\text{HLbL};\pi^0(2)} = \int_0^\infty dQ_1 \int_0^\infty dQ_2 \int_{-1}^1 d\tau w_2(Q_1, Q_2, \tau) \times \mathcal{F}_{\pi^0\gamma^*\gamma^*}(-Q_1^2, -Q_2^2) \mathcal{F}_{\pi^0\gamma^*\gamma^*}(-(Q_1 + Q_2)^2, 0). \quad (12)$$

The integrations in Eqs. (11) and (12) run over the lengths of the two Euclidean four-momenta Q_1 and Q_2 and the angle θ between them $Q_1 \cdot Q_2 = Q_1 Q_2 \cos \theta$. We have written $Q_i \equiv |(Q_i)_\mu|, i = 1, 2$, for the length of the four-vectors. Following Ref. [31] we changed the notation used in Ref. [2] and write $\tau = \cos \theta$ in order to avoid confusion with the Mandelstam variable t in the context of the dispersive approach.

The weight functions which appear in the integrals (11) and (12) are given by

$$w_1(Q_1, Q_2, \tau) = \left(-\frac{2\pi}{3}\right) \sqrt{1 - \tau^2} \frac{Q_1^3 Q_2^3}{Q_2^2 + m_\pi^2} I_1(Q_1, Q_2, \tau), \quad (13)$$

$$w_2(Q_1, Q_2, \tau) = \left(-\frac{2\pi}{3}\right) \sqrt{1 - \tau^2} \frac{Q_1^3 Q_2^3}{(Q_1 + Q_2)^2 + m_\pi^2} I_2(Q_1, Q_2, \tau), \quad (14)$$

where the functions $I_{1,2}(Q_1, Q_2, \tau)$ have been calculated in Ref. [2] and are given in Appendix A. From our definition of the form factor in Eq. (5) it follows that the weight functions $w_{1,2}(Q_1, Q_2, \tau)$ are dimensionless. Furthermore $w_2(Q_1, Q_2, \tau)$ is symmetric under $Q_1 \leftrightarrow Q_2$ [2]. Finally, $w_{1,2}(Q_1, Q_2, \tau) \rightarrow 0$ for $Q_{1,2} \rightarrow 0$ and for $\tau \rightarrow \pm 1$. The precise behavior of $w_{1,2}(Q_1, Q_2, \tau)$ for $Q_{1,2} \rightarrow 0$ and $\tau \rightarrow \pm 1$, as well as for $Q_{1,2} \rightarrow \infty$, can be found in Appendix A.

The three-dimensional integral representation in Eqs. (11) and (12) separates the generic kinematics in the pion-pole contribution to HLbL, described by the model-independent weight functions $w_{1,2}(Q_1, Q_2, \tau)$,³ from the dependence on the single- and

³Note that the weight functions $w_{1,2}(Q_1, Q_2, \tau)$ also describe the relevant momentum regions in the case where one defines the pion-pole contribution according to Refs. [22, 36] and sets the single-

double-virtual form factors $\mathcal{F}_{\pi^0\gamma^*\gamma^*}(-Q^2, 0)$ and $\mathcal{F}_{\pi^0\gamma^*\gamma^*}(-Q_1^2, -Q_2^2)$ in the spacelike (Euclidean) region, which can in principle be measured, obtained from a dispersion relation [44] (for η, η' in Refs. [45, 46, 47]), or, as has been done so far, modelled. We will discuss the experimental situation concerning the single- and double-virtual TFF of π^0, η, η' below in Section 5.

In Ref. [21] a two-dimensional integral representation for $a_\mu^{\text{HLbL};\pi^0}$ was derived which also allowed a separation between certain weight functions and the form factors, however, the derivation was only possible for a class of VMD-like form factors based on large- N_c QCD. The constant Wess-Zumino-Witten (WZW) [48] form factor, as defined in Eq. (B1), also falls into this class and since in this case there is no dependence on the angle θ from the form factors in Eqs. (11) and (12), one can obtain two of the weight functions in Ref. [21] from the weight functions derived in Ref. [2] by integrating over the angles

$$w_{f_1}(Q_1, Q_2) = \int_{-1}^1 d\tau w_1(Q_1, Q_2, \tau), \quad (15)$$

$$w_{g_2}(m_\pi, Q_1, Q_2)|_{\text{symm}} = \int_{-1}^1 d\tau w_2(Q_1, Q_2, \tau), \quad (16)$$

where $w_{g_2}(m_\pi, Q_1, Q_2)|_{\text{symm}} = [w_{g_2}(m_\pi, Q_1, Q_2) + w_{g_2}(m_\pi, Q_2, Q_1)]/2$. Only this symmetric part of the function $w_{g_2}(m_\pi, Q_1, Q_2)$ given in Ref. [21] contributes in the corresponding two-dimensional integral representation for $a_\mu^{\text{HLbL};\pi^0(2)}$ since it is multiplied by $\mathcal{F}_{\pi^0\gamma^*\gamma^*}(-Q_1^2, -Q_2^2)$. This symmetrization removes the negative regions visible in the plots for the function $w_{g_2}(m_\pi, Q_1, Q_2)$ shown in Ref. [21]. The plots of the symmetrized function will then look very similar to those for $w_2(Q_1, Q_2, \tau)$ shown in Fig. 2 below. We have checked the relations (15) and (16) numerically.

As one can see from the expressions for the weight functions $w_{1,2}$ in Eqs. (13) and (14), the only explicit dependence on the pseudoscalar appears via the mass in the pseudoscalar propagators. This will be important with respect to the most relevant momentum regions for the HLbL contribution to the muon $g - 2$. Of course, also the form factors will depend on the type of the pseudoscalar. First of all the normalization of the form factors is related to the decay width $\Gamma(P \rightarrow \gamma\gamma)$, and, secondly, there is a difference in the momentum dependence, since e.g. in a VMD model, the relevant vector meson masses will be different for π^0, η and η' (e.g. ρ -meson versus ϕ -meson).

3 Model-independent weight functions $w_{1,2}(Q_1, Q_2, \tau)$

3.1 Weight functions for π^0

In Fig. 2 we have plotted the weight functions $w_1(Q_1, Q_2, \tau)$ and $w_2(Q_1, Q_2, \tau)$ for the pion as function of Q_1 and Q_2 for a selection of values of θ . Note that although the weight

virtual form factor at the external vertex to a constant. Moreover, these weight functions are also relevant if one evaluates the pion-exchange contribution with model-dependent off-shell pion form factors $\mathcal{F}_{\pi^0\gamma^*\gamma^*}(-(Q_1 + Q_2)^2, -Q_1^2, -Q_2^2)$ [11, 2].

functions rise very quickly to the maxima in the plots in Figs. 2, the slopes along the two axis and along the diagonal $Q_1 = Q_2$ actually vanish for both functions, see Eq. (A21). We stress again that these weight functions are completely independent of any models for the form factors. In this respect these three-dimensional plots differ from similar plots in Ref. [49] which show, in the context of specific models, for various contributions to HLbL the full integrand in the (Q_1, Q_2) -plane after the angular integrations, including the form factors.

Table 2: Values of the maxima of the weight functions $w_1(Q_1, Q_2, \tau)$ and $w_2(Q_1, Q_2, \tau)$ for the pion and locations of the maxima in the (Q_1, Q_2) -plane for a selection of angles θ with decreasing θ (increasing $\tau = \cos \theta$).

θ ($\tau = \cos \theta$)	Max. w_1	Q_1 [GeV]	Q_2 [GeV]	Max. w_2	$Q_1 = Q_2$ [GeV]
175° (-0.996)	0.592	0.163	0.163	0.100	0.142
165° (-0.966)	1.734	0.164	0.162	0.277	0.132
150° (-0.866)	3.197	0.166	0.158	0.441	0.114
135° (-0.707)	4.176	0.171	0.153	0.494	0.099
120° (-0.5)	4.559	0.176	0.146	0.471	0.087
105° (-0.259)	4.349	0.182	0.139	0.403	0.078
90° (0.0)	3.664	0.187	0.130	0.312	0.070
75° (0.259)	2.702	0.189	0.122	0.218	0.063
60° (0.5)	1.691	0.187	0.114	0.132	0.057
45° (0.707)	0.840	0.180	0.106	0.064	0.050
30° (0.866)	0.283	0.168	0.099	0.021	0.043
15° (0.966)	0.0385	0.154	0.092	0.0027	0.037
5° (0.996)	0.0015	0.147	0.089	0.000092	0.037

We can immediately see that for both weight functions the low-momentum region, $Q_{1,2} \leq 0.5$ GeV, is the most important in the corresponding integrals (11) and (12) for $a_\mu^{\text{HLbL};\pi^0}$. For $w_1(Q_1, Q_2, \tau)$ there is a peak around $Q_1 \sim 0.15 - 0.19$ GeV, $Q_2 \sim 0.09 - 0.16$ GeV. In Table 2 we have collected the values of the maxima of $w_1(Q_1, Q_2, \tau)$ and the locations of the maxima in the (Q_1, Q_2) -plane for a selection of values of θ . With decreasing θ (increasing τ), the value of the maximum grows until $\theta = 120^\circ$ ($\tau = -0.5$) and then decreases again. Note that $w_1(Q_1, Q_2, \tau)$ can become negative for $\theta \leq 75^\circ$ and for some values of $Q_{1,2}$, but the minima are small in absolute size compared to the maxima. Table 3 shows the global maximum and minimum of the function $w_1(Q_1, Q_2, \tau)$ in the physically allowed region $Q_{1,2} \geq 0$ and $-1 \leq \tau \leq 1$.

For $\theta \leq 150^\circ$ ($\tau \geq -0.85$), a ridge develops along the Q_1 direction for $Q_2 \sim 0.18 - 0.26$ GeV (maximum along the line $Q_1 = 2$ GeV). This ridge leads for a constant WZW

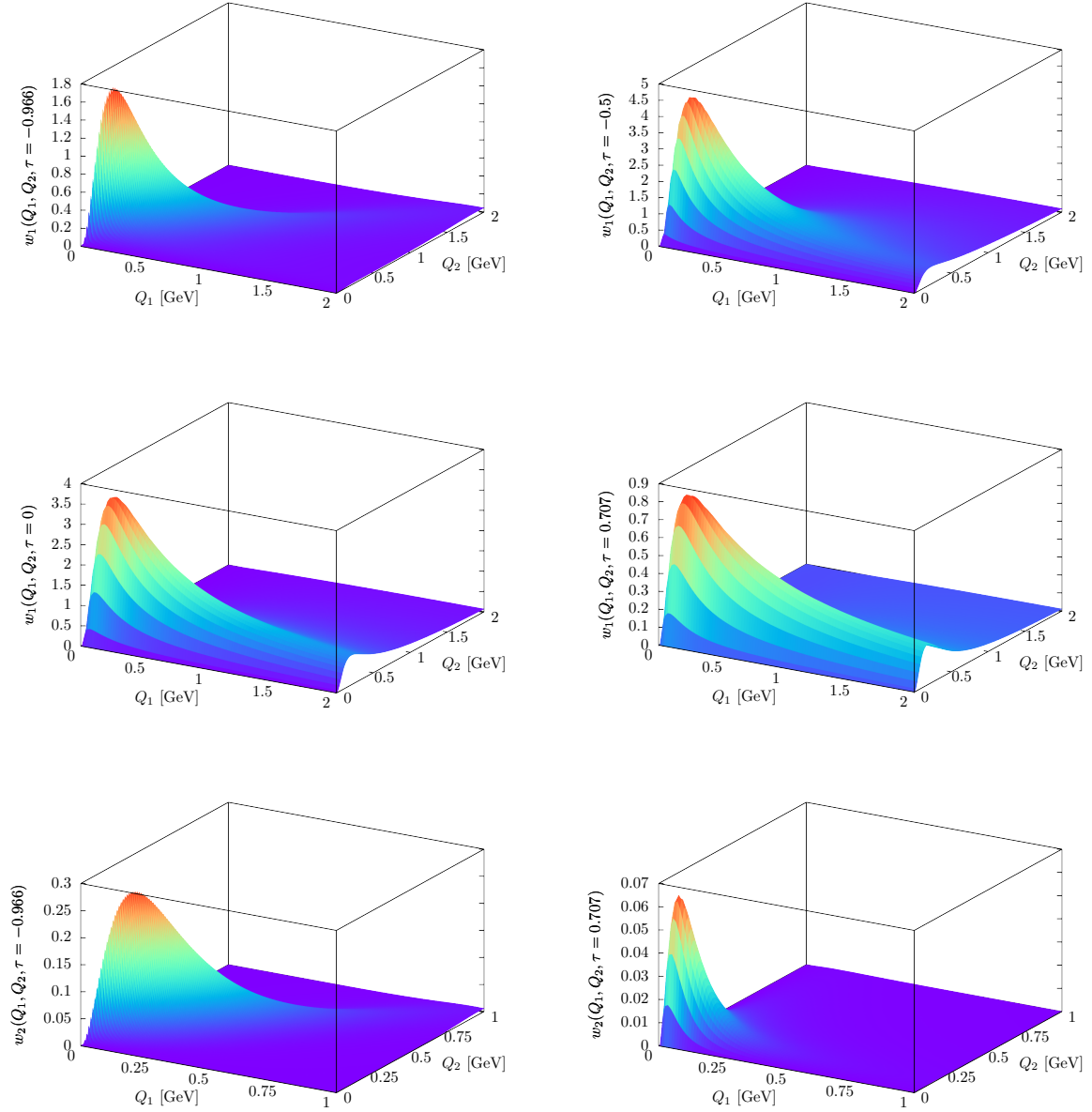


Figure 2: Weight functions $w_1(Q_1, Q_2, \tau)$ and $w_2(Q_1, Q_2, \tau)$ for the pion as function of the Euclidean momenta Q_1 and Q_2 for a selection of values of $\tau = \cos \theta$. Top left: w_1 for $\theta = 165^\circ$ ($\tau = -0.966$), top right: w_1 for $\theta = 120^\circ$ ($\tau = -0.5$), middle left: w_1 for $\theta = 90^\circ$ ($\tau = 0$), middle right: w_1 for $\theta = 45^\circ$ ($\tau = 0.707$). Bottom left: w_2 for $\theta = 165^\circ$ ($\tau = -0.966$), bottom right: w_2 for $\theta = 45^\circ$ ($\tau = 0.707$). Note the different range in $Q_{1,2}$ for w_2 . The plots of w_2 for $\theta = 120^\circ$ and 90° look similar to the one shown for $\theta = 45^\circ$, but the peaks are slightly broader.

Table 3: Values and locations in (Q_1, Q_2, θ) of the global maxima and minima of the weight functions $w_1(Q_1, Q_2, \tau)$ and the global maxima of $w_2(Q_1, Q_2, \tau)$ for all three pseudoscalars π^0, η, η' .

	Value	Q_1 [GeV]	Q_2 [GeV]	θ ($\tau = \cos \theta$)
Max. $w_1 _{\pi^0}$	4.563	0.177	0.145	118.1° (-0.471)
Min. $w_1 _{\pi^0}$	-0.0044	0.118	1.207	45.7° (0.698)
Max. $w_2 _{\pi^0}$	0.495	0.097	0.097	133.1° (-0.684)
Max. $w_1 _{\eta}$	0.813	0.322	0.310	123.8° (-0.556)
Min. $w_1 _{\eta}$	-0.0037	0.129	1.368	47.1° (0.680)
Max. $w_2 _{\eta}$	0.044	0.124	0.124	122.0° (-0.531)
Max. $w_1 _{\eta'}$	0.332	0.415	0.416	124.8° (-0.571)
Min. $w_1 _{\eta'}$	-0.0030	0.144	1.595	48.7° (0.661)
Max. $w_2 _{\eta'}$	0.015	0.128	0.128	120.9° (-0.513)

form factor to an ultraviolet divergence $(\alpha/\pi)^3 \mathcal{C} \ln^2(\Lambda/m_\mu)$ [50] for some momentum cutoff Λ with $\mathcal{C} = 3(N_c/(12\pi))^2(m_\mu/F_\pi)^2 = 0.0248$ [21, 51]. Of course, realistic form factors fall off for large momenta $Q_{1,2}$, see Fig. 7 in Appendix B, and the integral $a_\mu^{\text{HLbL};\pi^0(1)}$ will be convergent.

The weight function $w_2(Q_1, Q_2, \tau)$ is about an order of magnitude smaller than $w_1(Q_1, Q_2, \tau)$ as can be seen in Fig. 2. There is no ridge, since the function is symmetric under $Q_1 \leftrightarrow Q_2$. Here the peak is around $Q_1 = Q_2 \sim 0.14$ GeV for τ near -1 . The value of the maximum grows for decreasing θ (increasing τ), until $\theta = 135^\circ$ ($\tau = -0.707$) and then decreases again. The location of the peak thereby moves to much lower values, down to $Q_1 = Q_2 \sim 0.04$ GeV when τ is near $+1$, see Table 2 for more details about the peak locations. The function $w_2(Q_1, Q_2, \tau)$ is always positive and its global maximum is shown in Table 3.

Figure 3 shows the weight functions $w_{1,2}(Q_1, Q_2, \tau)$ as a function of τ for some selected values of Q_1 and Q_2 . One can see that there is a strong enhancement for $Q_1 = Q_2$ for negative τ when the original four-vectors $(Q_1)_\mu$ and $(Q_2)_\mu$ become more and more antiparallel. In particular, the functions have a rather large slope for $\tau \rightarrow -1$ and the maximal value is always located at $\tau < 0$.⁴ However, both weight functions always vanish for $\tau = -1$, as mentioned before and discussed in Appendix A. Furthermore the weight functions get smaller for growing values of $Q_{1,2} > 0.5$ GeV, as is already visible in the three-dimensional plots in Fig. 2.

⁴Note the factor $1/(Q_1 + Q_2)^2$ from one of the photon propagators in the weight functions $w_{1,2}(Q_1, Q_2, \tau)$, see Eqs. (A5) and (A6). According to Eqs. (A31) and (A35) the weight functions $w_{1,2}(Q, Q, \tau)$ along the diagonal $Q_1 = Q_2 = Q$ have infinite slope at $\tau = -1$.

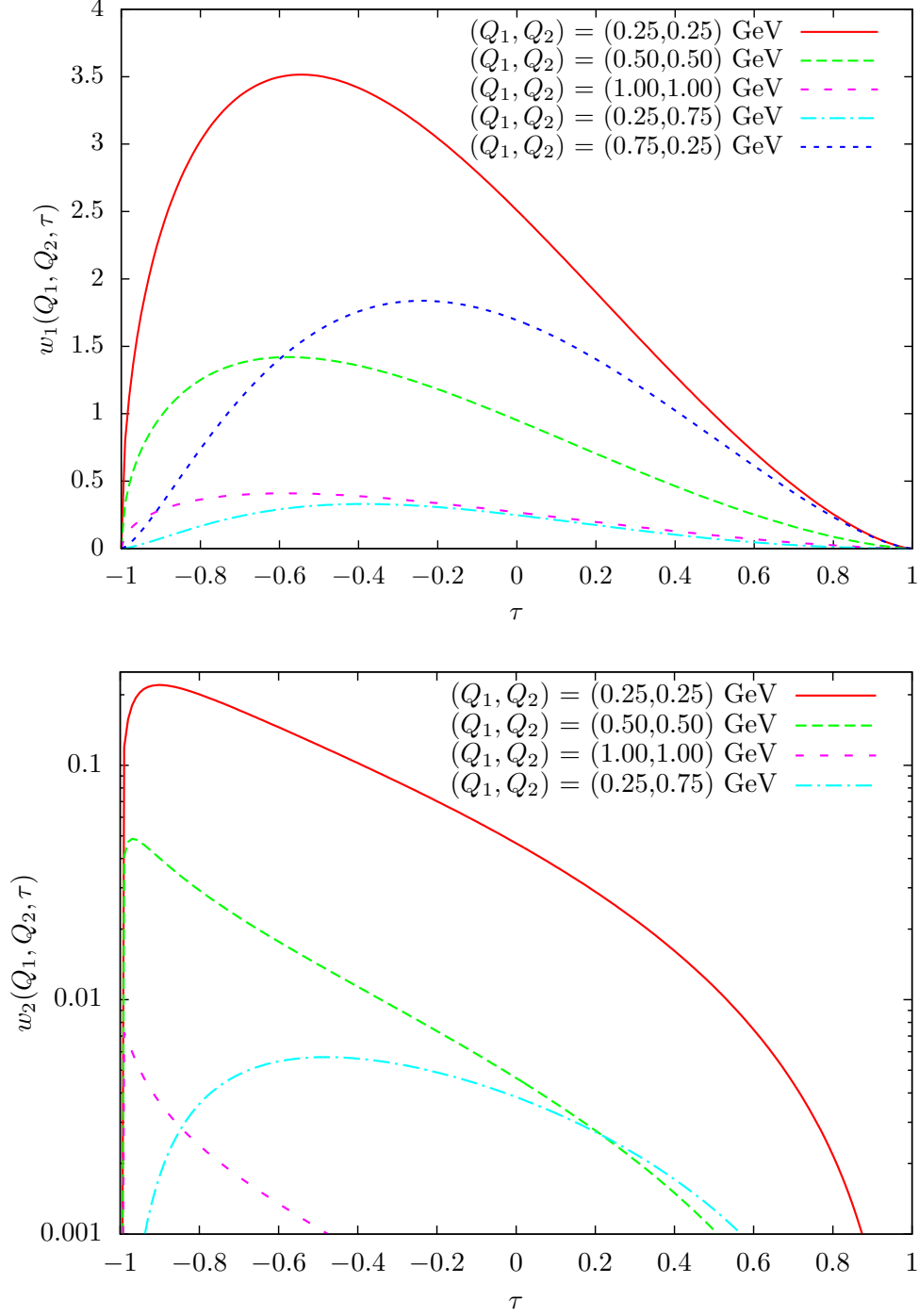


Figure 3: Weight functions $w_1(Q_1, Q_2, \tau)$ (top) and $w_2(Q_1, Q_2, \tau)$ (bottom) for the pion as function of $\tau = \cos \theta$ for a selection of Q_1 and Q_2 values. Note the logarithmic scale for w_2 and that the function is symmetric under the exchange $Q_1 \leftrightarrow Q_2$.

3.2 Weight functions for η and η'

In Fig. 4 we have plotted the model-independent weight functions $w_{1,2}(Q_1, Q_2, \tau)$ for the η and the η' as a function of Q_1 and Q_2 for the two angles $\theta = 165^\circ$ and 45° . The shape of the plots for $\theta = 120^\circ$ and 90° is similar to the ones shown for $\theta = 45^\circ$.

The only dependence on the pseudoscalars appears in the weight functions $w_{1,2}(Q_1, Q_2, \tau)$ through the pseudoscalar propagators, i.e. a factor $1/(Q_2^2 + m_P^2)$ in w_1 and a factor $1/((Q_1 + Q_2)^2 + m_P^2) = 1/(Q_1^2 + 2Q_1Q_2\tau + Q_2^2 + m_P^2)$ in w_2 , see Eqs. (13) and (14). As can be seen from the plots in Fig. 4, this shifts the relevant momentum regions (peaks, ridges) in the weight functions to higher momenta for η compared to π^0 and even higher for η' . Note that for w_1 the momentum range in the plots for η and η' is now $0 - 3$ GeV, whereas it was only $0 - 2$ GeV for π^0 in Fig. 2. It also leads to a suppression in the absolute size of the weight functions due to the larger masses in the propagators. This pattern will also be visible in the values for the contributions to HLbL. For the bulk of the weight functions (maxima, ridges) we observe the following approximate relations (for the same angle θ , but not necessarily at the same values of the momenta)

$$w_1|_\eta \approx \frac{1}{6} w_1|_{\pi^0}, \quad (17)$$

$$w_1|_{\eta'} \approx \frac{1}{2.5} w_1|_\eta. \quad (18)$$

Of course, the ratio of the weight functions is given by the ratio of the propagators and is maximal at zero momenta and at that point equal to the ratio of the squares of the masses, but at zero momenta the weight functions themselves vanish. The combined effect is well described by the relations in Eqs. (17) and (18). Furthermore, for both η and η' , the weight function w_2 is about a factor 20 smaller than the corresponding weight function w_1 .

The peaks for the weight function $w_1(Q_1, Q_2, \tau)$ for η and η' are less steep, compared to π^0 , and the ridge is quite broad in the Q_2 -direction. Furthermore, the ridge falls off only slowly in the Q_1 -direction and for $\theta \leq 75^\circ$ is still about half of the maximum out to values of $Q_1 = 3$ GeV. For the weight function $w_2(Q_1, Q_2, \tau)$ the peaks are again less steep and larger values of the momenta contribute, compared to the pion.

Table 4 shows for η and η' the maxima of the weight functions $w_{1,2}(Q_1, Q_2, \tau)$ and the locations of the maxima in the (Q_1, Q_2) -plane for a selection of angles θ . For the η -meson, the peak in the weight function $w_1(Q_1, Q_2, \tau)$ is around $Q_1 \sim 0.32 - 0.37$ GeV, $Q_2 \sim 0.22 - 0.33$ GeV. For $\theta \leq 120^\circ$ ($\tau \geq -0.5$), again the broad ridge along the Q_1 direction is visible with $Q_2 \sim 0.4 - 0.7$ GeV (maximum along the line $Q_1 = 2$ GeV). The peak for the weight function $w_2(Q_1, Q_2, \tau)$ is around $Q_1 = Q_2 \sim 0.14$ GeV for τ near -1 as for the pion. The location of the peak moves down to $Q_1 = Q_2 \sim 0.06$ GeV when τ is near $+1$. The global maximum and minimum of $w_1(Q_1, Q_2, \tau)$ and the global maximum of $w_2(Q_1, Q_2, \tau)$ are shown in Table 3.

For the η' , the peak in $w_1(Q_1, Q_2, \tau)$ now occurs for even higher momenta, $Q_1 \sim 0.41 - 0.51$ GeV, $Q_2 \sim 0.31 - 0.43$ GeV. Here the broad ridge along the Q_1 direction arises for $\theta \leq 120^\circ$ ($\tau \geq -0.5$) with $Q_2 \sim 0.6 - 1$ GeV. The locations of the peaks of

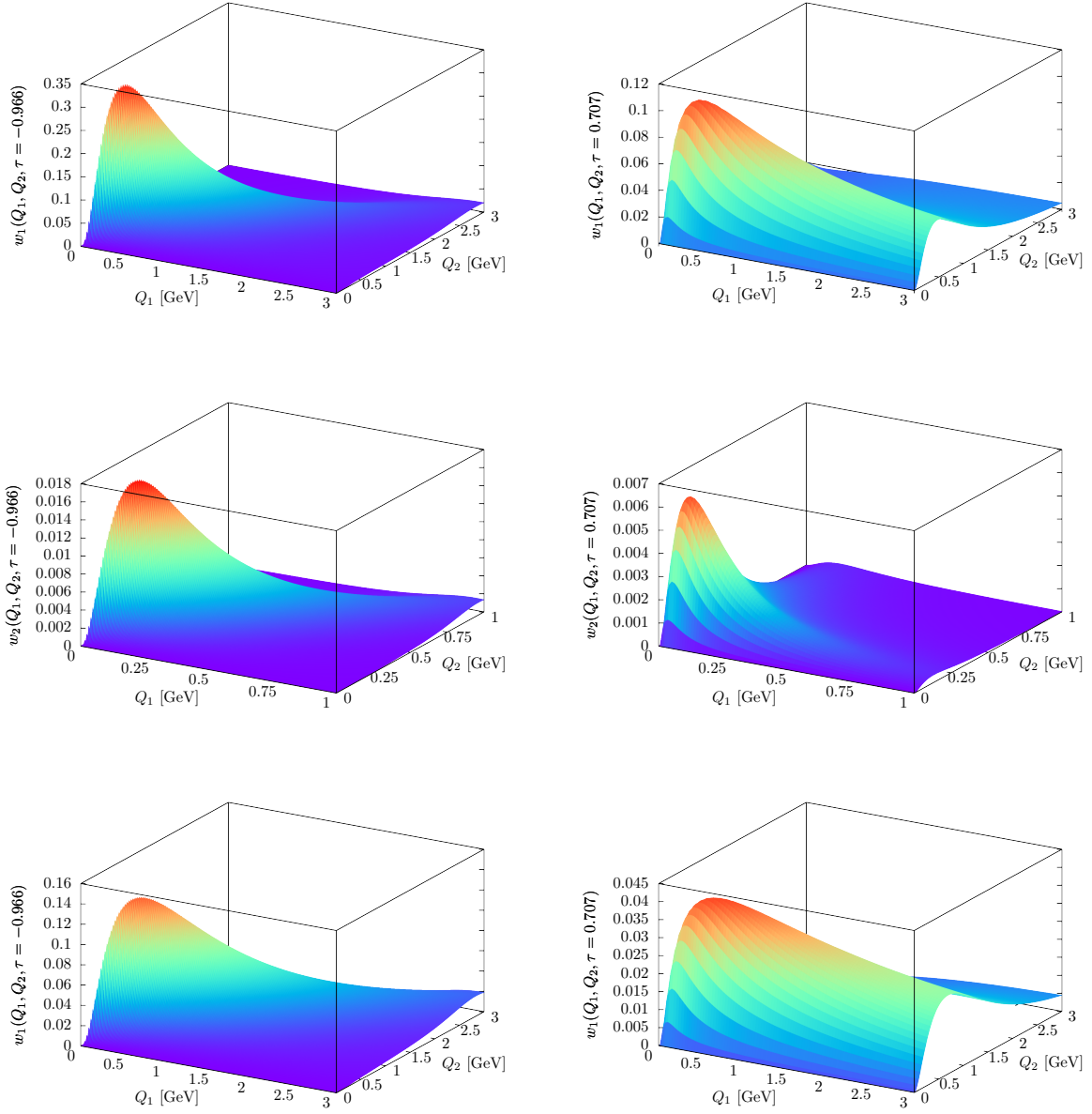


Figure 4: Weight functions $w_1(Q_1, Q_2, \tau)$ and $w_2(Q_1, Q_2, \tau)$ for the η and η' as function of the Euclidean momenta Q_1 and Q_2 , each for two values of $\tau = \cos \theta$. Top left: w_1 for η with $\theta = 165^\circ$ ($\tau = -0.966$), top right: w_1 for η with $\theta = 45^\circ$ ($\tau = 0.707$), middle left: w_2 for η with $\theta = 165^\circ$ ($\tau = -0.966$), middle right: w_2 for η with $\theta = 45^\circ$ ($\tau = 0.707$). Note the different range in $Q_{1,2}$ for w_2 . Bottom left: w_1 for η' with $\theta = 165^\circ$ ($\tau = -0.966$), bottom right: w_1 for η' with $\theta = 45^\circ$ ($\tau = 0.707$). The plots of w_2 for η' look similar to those for η with the same θ .

Table 4: Values of the maxima of the weight functions $w_{1,2}(Q_1, Q_2, \tau)$ and locations of the maxima in the (Q_1, Q_2) -plane for a selection of angles θ . Top part: η -meson. Bottom part: η' -meson.

θ ($\tau = \cos \theta$)	Max. w_1	Q_1 [GeV]	Q_2 [GeV]	Max. w_2	$Q_1 = Q_2$ [GeV]
175° (-0.996)	0.117	0.328	0.328	0.0061	0.143
165° (-0.966)	0.341	0.327	0.327	0.018	0.142
150° (-0.866)	0.616	0.325	0.323	0.032	0.137
135° (-0.707)	0.778	0.323	0.317	0.041	0.131
120° (-0.5)	0.809	0.322	0.308	0.044	0.123
105° (-0.259)	0.729	0.323	0.296	0.040	0.114
90° (0.0)	0.575	0.328	0.282	0.032	0.106
75° (0.259)	0.395	0.336	0.267	0.023	0.096
60° (0.5)	0.231	0.346	0.253	0.014	0.087
45° (0.707)	0.107	0.356	0.241	0.0063	0.077
30° (0.866)	0.034	0.363	0.231	0.0019	0.067
15° (0.966)	0.0044	0.367	0.225	0.00023	0.063
5° (0.996)	0.00017	0.368	0.224	8×10^{-6}	0.065
175° (-0.996)	0.049	0.434	0.434	0.0020	0.143
165° (-0.966)	0.142	0.432	0.433	0.0059	0.142
150° (-0.866)	0.255	0.427	0.430	0.011	0.139
135° (-0.707)	0.320	0.419	0.423	0.014	0.134
120° (-0.5)	0.330	0.413	0.412	0.015	0.128
105° (-0.259)	0.293	0.412	0.397	0.014	0.120
90° (0.0)	0.227	0.418	0.378	0.011	0.112
75° (0.259)	0.154	0.431	0.358	0.0079	0.102
60° (0.5)	0.088	0.451	0.340	0.0047	0.092
45° (0.707)	0.041	0.472	0.326	0.0022	0.082
30° (0.866)	0.013	0.491	0.315	0.00066	0.072
15° (0.966)	0.0017	0.504	0.309	0.000079	0.067
5° (0.996)	0.000062	0.508	0.307	3×10^{-6}	0.070

$w_2(Q_1, Q_2, \tau)$ in the (Q_1, Q_2) -plane follow a similar pattern as for the η meson, see Table 4. Again the global maximum and minimum of $w_1(Q_1, Q_2, \tau)$ and the global maximum of

$w_2(Q_1, Q_2, \tau)$ have been collected in Table 3.

4 Relevant momentum regions in $a_\mu^{\text{HLbL};\text{P}}$

In order to study the impact of different momentum regions on the pseudoscalar-pole contribution, we need, at least for the integral with the weight function $w_1(Q_1, Q_2, \tau)$ in Eq. (11), some knowledge on the form factor $\mathcal{F}_{\pi^0\gamma^*\gamma^*}(-Q_1^2, -Q_2^2)$, since the integral diverges for a constant form factor.⁵ For illustration we take for the pion two simple models to perform the integrals: Lowest Meson Dominance with an additional vector multiplet, LMD+V model [52, 21], based on the Minimal Hadronic Approximation [53, 54] to large- N_c QCD matched to certain QCD short-distance constraints from the operator product expansion (OPE) [55], and the well-known and often used VMD model. Of course, in the end, the models have to be replaced as much as possible by experimental data on the single- and double-virtual TFF or one can use a DR for the form factor itself [44, 45, 46, 47].

Some details and properties of these two form factor models can be found in Appendix B. There are two main differences between the models. First, the LMD+V model does not factorize $\mathcal{F}_{\pi^0\gamma^*\gamma^*}^{\text{LMD+V}}(-Q_1^2, -Q_2^2) \neq f(Q_1^2) \times f(Q_2^2)$. Such a factorization is also not expected in QCD. Second, the two models have a different behavior of the double-virtual form factor for large and equal momenta. The LMD+V model reproduces by construction the OPE [56, 57], whereas the VMD form factor falls off too fast (see Eq. (B2) for the exact OPE behavior):

$$\mathcal{F}_{\pi^0\gamma^*\gamma^*}^{\text{LMD+V}}(-Q^2, -Q^2) \sim \mathcal{F}_{\pi^0\gamma^*\gamma^*}^{\text{OPE}}(-Q^2, -Q^2) \sim \frac{1}{Q^2}, \quad \text{for large } Q^2, \quad (19)$$

$$\mathcal{F}_{\pi^0\gamma^*\gamma^*}^{\text{VMD}}(-Q^2, -Q^2) \sim \frac{1}{Q^4}, \quad \text{for large } Q^2. \quad (20)$$

Nevertheless, as can be seen from Fig. 7 and Table 8 in Appendix B, for not too large momenta, $Q_1 = Q_2 = Q = 0.5$ [0.75] GeV, the form factors $\mathcal{F}_{\pi^0\gamma^*\gamma^*}(-Q^2, -Q^2)$ in the two models differ by only 3% [10%]. Furthermore, both models give an equally good description of the single-virtual TFF $\mathcal{F}_{\pi^0\gamma^*\gamma^*}(-Q^2, 0)$ [52, 58].

The LMD+V model was developed in Ref. [52] in the chiral limit and assuming octet symmetry. This is certainly not a good approximation for the more massive η and η' mesons, where also the nonet symmetry, the effect of the $U(1)_A$ anomaly and the $\eta - \eta'$ -mixing have to be taken into account. Since we are interested here in the determination of the relevant momentum regions of the pseudoscalar-pole contributions to HLbL and the impact of experimental measurement errors of the form factors, we will take for the η and η' mesons the usual VMD model for the TFF, as already done in Refs. [21, 11]. See Appendix B for more details about the VMD model parameters for η and η' .

⁵As already observed in Refs. [19, 21], for the integral with the weight function $w_2(Q_1, Q_2, \tau)$ in Eq. (12) one obtains even for a constant WZW form factor a finite and small result: $(\frac{\alpha}{\pi})^3 a_{\mu; \text{WZW}}^{\text{HLbL}; \pi^0(2)} = 2.5 \times 10^{-11}$, $(\frac{\alpha}{\pi})^3 a_{\mu; \text{WZW}}^{\text{HLbL}; \eta(2)} = 0.78 \times 10^{-11}$ and $(\frac{\alpha}{\pi})^3 a_{\mu; \text{WZW}}^{\text{HLbL}; \eta'(2)} = 0.65 \times 10^{-11}$.

The two models yield the following results for the pole-contributions of the light pseudoscalars to HLbL (we list here only the central values)⁶

$$a_{\mu;\text{LMD+V}}^{\text{HLbL};\pi^0} = 62.9 \times 10^{-11}, \quad (21)$$

$$a_{\mu;\text{VMD}}^{\text{HLbL};\pi^0} = 57.0 \times 10^{-11}, \quad (22)$$

$$a_{\mu;\text{VMD}}^{\text{HLbL};\eta} = 14.5 \times 10^{-11}, \quad (23)$$

$$a_{\mu;\text{VMD}}^{\text{HLbL};\eta'} = 12.5 \times 10^{-11}. \quad (24)$$

The results (21) and (22) for the pion-pole contribution in the two models are in the ballpark of many other estimates, see Eq. (9), but they also differ by 9.4%, relative to the LMD+V result, due to the different high-energy behavior for the double-virtual TFF in Eqs. (19) and (20) for $Q_{1,2} \geq 1$ GeV. In fact, the pattern of the contributions to $a_{\mu}^{\text{HLbL};\pi^0}$ is to a large extent determined by the model-independent weight functions $w_{1,2}(Q_1, Q_2, \tau)$, which are concentrated below about 0.5 GeV, up to that ridge in w_1 along the Q_1 direction. As long as realistic form factor models for the double-virtual case fall off at large momenta and do not differ too much at low momenta (with the normalization from $\Gamma(\pi^0 \rightarrow \gamma\gamma)$ and constraints from the single-virtual transition form factor), we expect similar results for the pion-pole contribution at the level of 15% which is in fact what is seen in the literature [37]. Nevertheless, due to the ridge-like structure in the weight function w_1 along the Q_1 direction, the high-energy behavior of the form factors is relevant at the precision of 10% one is aiming for.

For the η and η' , the results in Eqs. (23) and (24) are as expected from the discussion of the relative size of the weight functions in Eqs. (17) and (18). The result for η is about a factor 4 smaller than for the pion with VMD. The result for η' is only slightly smaller than for η . Note that the normalization of the form factors related to the decay $\Gamma(P \rightarrow \gamma\gamma)$ and the momentum dependence due to different values of M_V for η and η' also play an important role for the results in Eqs. (23) and (24).

For a more detailed analysis, we integrate in Eqs. (11) and (12) over individual momentum bins and all angles θ as follows

$$\int_{Q_{1,\min}}^{Q_{1,\max}} dQ_1 \int_{Q_{2,\min}}^{Q_{2,\max}} dQ_2 \int_{-1}^1 d\tau \quad (25)$$

and display the results, relative to the totals in Eqs. (21)-(24), in Fig. 5.

Since the absolute size of the weight function $w_1(Q_1, Q_2, \tau)$ is much larger than $w_2(Q_1, Q_2, \tau)$, the contribution from the integral $a_{\mu}^{\text{HLbL};P(1)}$ in Eq. (11) dominates over $a_{\mu}^{\text{HLbL};P(2)}$ in Eq. (12). Therefore the asymmetry seen in the (Q_1, Q_2) -plane in Fig. 5, with larger contributions below the diagonal, reflects the ridge-like structure of $w_1(Q_1, Q_2, \tau)$

⁶ Although the weight functions $w_{1,2}(Q_1, Q_2, \tau)$ vanish for $Q_{1,2} \rightarrow 0$ and $\tau \rightarrow \pm 1$, for the numerical integration with VEGAS [59] we introduced a small infrared / collinear cutoff as follows: $Q_{1,2} \geq \epsilon$ GeV, $\tau \leq 1 - \epsilon$ and $\tau \geq -1 + \epsilon^2$ with $\epsilon = 10^{-6}$, where the latter condition takes into account the steeper slope for $\tau \rightarrow -1$, when $Q_1 = Q_2$, see Fig. 3 and Eqs. (A31) and (A35) in Appendix A.

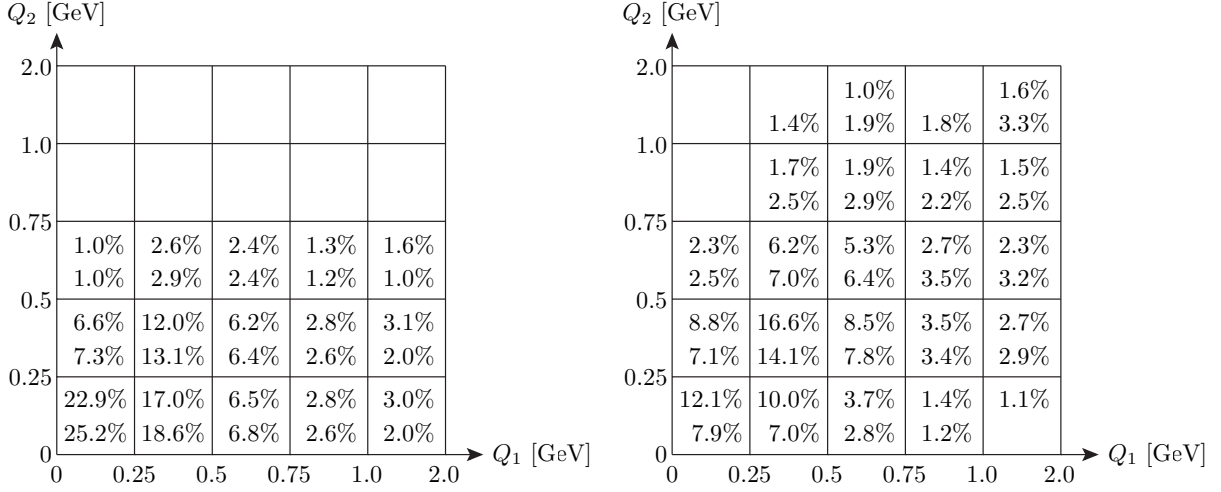


Figure 5: Left panel: Relative contributions to the total $a_\mu^{\text{HLbL};\pi^0}$ from individual bins in the (Q_1, Q_2) -plane, integrated over all angles according to Eq. (25). Note the larger size of the bins with $Q_{1,2} \geq 1$ GeV. Top line in each bin: LMD+V model, bottom line: VMD model. Contributions smaller than 1% have not been displayed. For the LMD+V model there are further contributions bigger than 1% along the Q_1 -axis. For $2 \text{ GeV} \leq Q_1 \leq 20 \text{ GeV}$: 1.1% in the bin $0 \leq Q_2 \leq 0.25$ GeV and 1.2% for $0.25 \text{ GeV} \leq Q_2 \leq 0.5$ GeV. Right panel: Relative contributions to the total of $a_\mu^{\text{HLbL};\eta}$ and $a_\mu^{\text{HLbL};\eta'}$ with the VMD model from individual bins in the (Q_1, Q_2) -plane, integrated over all angles. Top line in each bin: η -meson, bottom line: η' -meson.

in Figs. 2 and 4. Note that in relating the contributions to $a_\mu^{\text{HLbL};\text{P}}$ from different momentum regions to the form factor, one has to take into account that what enters in the dominant part $a_\mu^{\text{HLbL};\text{P}(1)}$ in Eq. (11) is the double-offshell form factor at momenta $\mathcal{F}_{\text{P}\gamma^*\gamma^*}(-Q_1^2, -(Q_1 + Q_2)^2)$, not $\mathcal{F}_{\text{P}\gamma^*\gamma^*}(-Q_1^2, -Q_2^2)$.

For the pion, the largest contribution comes from the lowest bin $Q_{1,2} \leq 0.25$ GeV since a large part of the peaks in the weight functions (for different angles θ) is contained in that bin. More than half of the contribution comes from the four bins with $Q_{1,2} \leq 0.5$ GeV. In contrast, for the η and η' , it is not the bin $Q_{1,2} \leq 0.25$ GeV which yields the largest contribution, since the maxima of the weight functions are shifted to higher momenta, around $0.3 - 0.5$ GeV. Furthermore, more bins up to $Q_2 = 2$ GeV now contribute at least 1% to the total. This is different from the pattern seen for π^0 . The plots of the weight functions for η and η' in Figs. 4 show that now the region $1.5 - 2.5$ GeV is also important for the evaluation of the η - and η' -pole contributions. However, as mentioned before, the VMD model is known to have a too fast fall-off at large momenta, compared to the OPE. Therefore the size of the contributions $a_\mu^{\text{HLbL};\eta}$ and $a_\mu^{\text{HLbL};\eta'}$ in Eqs. (23) and (24) might be underestimated by the VMD model, which could also affect the relative importance of the higher momentum region in Fig. 5.

Integrating both Q_1 and Q_2 from zero up to some upper momentum cutoff Λ (inte-

Table 5: Pseudoscalar-pole contribution $a_\mu^{\text{HLbL};P} \times 10^{11}$, $P = \pi^0, \eta, \eta'$, for different form factor models obtained with a momentum cutoff Λ . In brackets, relative contribution of the total obtained with $\Lambda = 20$ GeV.

Λ [GeV]	π^0 [LMD+V]	π^0 [VMD]	η [VMD]	η' [VMD]
0.25	14.4 (22.9%)	14.4 (25.2%)	1.8 (12.1%)	1.0 (7.9%)
0.5	36.8 (58.5%)	36.6 (64.2%)	6.9 (47.5%)	4.5 (36.1%)
0.75	48.5 (77.1%)	47.7 (83.8%)	10.7 (73.4%)	7.8 (62.5%)
1.0	54.1 (86.0%)	52.6 (92.3%)	12.6 (86.6%)	9.9 (79.1%)
1.5	58.8 (93.4%)	55.8 (97.8%)	14.0 (96.1%)	11.7 (93.1%)
2.0	60.5 (96.2%)	56.5 (99.2%)	14.3 (98.6%)	12.2 (97.4%)
5.0	62.5 (99.4%)	56.9 (99.9%)	14.5 (100%)	12.5 (99.9%)
20.0	62.9 (100%)	57.0 (100%)	14.5 (100%)	12.5 (100%)

gration over a square) and integrating over all angles θ , one obtains the results shown in Table 5, see also Ref. [60] for a similar analysis for the pseudoscalar-exchange contribution. This amounts to summing up the individual bins shown in Fig. 5.

As one can see in Table 5, for the pion more than half of the final result stems from the region below $\Lambda = 0.5$ GeV (59% for LMD+V, 64% for VMD) and the region below $\Lambda = 1$ GeV gives the bulk of the total result (86% for LMD+V, 92% for VMD). The small difference between the form factor models for small momenta $Q_{1,2} \leq 0.5$ GeV is reflected in the small absolute difference for $a_\mu^{\text{HLbL};\pi^0}$ in the two models for $\Lambda \leq 0.75$ GeV. For instance, for $\Lambda = 0.5$ GeV, the difference is only 0.2×10^{-11} , i.e. about 0.5% and for $\Lambda = 0.75$ GeV, the difference is only 0.8×10^{-11} , i.e. 1.6%. The faster fall-off of the VMD model at larger momenta beyond 1 GeV, compared to the LMD+V model, leads to a smaller contribution from that region to the total. Therefore we can see in Fig. 5 that the main contributions in the VMD model, relative to the total, are concentrated at lower momenta, compared to the LMD+V model, in particular below 0.75 GeV.

On the other hand, Table 5 shows that for η and η' , the region below $\Lambda = 0.25$ GeV only gives a small contribution to the total (12% for η , 8% for η'). Up to $\Lambda = 0.5$ GeV, we get about half (one third) for η (η') and the bulk of the results comes from the region below $\Lambda = 1.5$ GeV, 96% for the η and 93% for the η' -meson. But note again, that the VMD model might have a too strong fall-off at large momenta. A less model-dependent evaluation of $a_\mu^{\text{HLbL};\eta}$ and $a_\mu^{\text{HLbL};\eta'}$, largely based on experimental data, would therefore be highly preferable.

5 Experimental status of transition form factors

For the calculation of the pseudoscalar-pole contribution $a_\mu^{\text{HLbL};P}$ with $P = \pi^0, \eta, \eta'$ in Eqs. (11) and (12) the single-virtual form factor $\mathcal{F}_{P\gamma^*\gamma^*}(-Q^2, 0)$ and the double-virtual

form factor $\mathcal{F}_{P\gamma^*\gamma^*}(-Q_1^2, -Q_2^2)$, both in the spacelike region, enter. We are interested here in the impact of uncertainties of experimental measurements of these form factors on the precision of $a_\mu^{\text{HLbL;P}}$. In the following, we will summarize the experimental information which is currently available for these form factors or which should be available in the near future. We will mostly just quote the uncertainties of several experiments in different momentum regions, concentrating on the most precise and most recent ones. More details about the actual measurements can be found in the given references. See Ref. [33] for a brief overview of the various experimental processes where information on the transition form factors can be obtained. More details can be found in Ref. [34].

For the single-virtual form factor we parametrize the measurement errors in Eqs. (11) and (12) as follows:

$$\mathcal{F}_{P\gamma^*\gamma^*}(-Q^2, 0) \rightarrow \mathcal{F}_{P\gamma^*\gamma^*}(-Q^2, 0) (1 \pm \delta_{1,P}(Q)). \quad (26)$$

The momentum dependent errors $\delta_{1,P}(Q)$ in different bins are displayed in Table 6 in Section 6. Ideally, one should combine all the experimental data to obtain $\mathcal{F}_{P\gamma^*\gamma^*}(-Q^2, 0)$ and $\delta_{1,P}(Q)$ as function for all momenta. However, there are currently still regions where there are no or rather unprecise data available. We therefore need to make some assumptions and will employ a simplified approach with bin-wise constant errors. Also, no correlations between different bins are taken into account.

Similarly, for the double-virtual form factor we parametrize the measurement errors in the following way

$$\mathcal{F}_{P\gamma^*\gamma^*}(-Q_1^2, -Q_2^2) \rightarrow \mathcal{F}_{P\gamma^*\gamma^*}(-Q_1^2, -Q_2^2) (1 \pm \delta_{2,P}(Q_1, Q_2)), \quad (27)$$

where the assumed momentum dependent errors $\delta_{2,P}(Q_1, Q_2)$ in different bins are shown in Fig. 6 in Section 6. Since there are currently no data available for the double-offshell form factor, we will use the results of a MC simulation [42] for BESIII, as described below, to estimate the errors $\delta_{2,P}(Q_1, Q_2)$.

5.1 Pion transition form factor

For the single-virtual TFF of the pion $\mathcal{F}_{\pi^0\gamma^*\gamma^*}(-Q^2, 0)$ the following experimental information is available. The normalization of the form factor can be obtained from the decay width $\Gamma(\pi^0 \rightarrow \gamma\gamma) = (\pi\alpha^2 m_\pi^3/4) \mathcal{F}_{\pi^0\gamma^*\gamma^*}^2(0, 0)$. For a detailed overview of theory and experiment we refer to Ref. [61]. See also Ref. [62] which briefly reviews the theory for other decay modes of the neutral pion that will be discussed below. From the Particle Data Group (PDG) average [4] for the decay width $\Gamma(\pi^0 \rightarrow \gamma\gamma) = (7.63 \pm 0.16) \text{ eV}$, one obtains a 1.1% precision on the form factor normalization. The error is largely driven by the single most precise measurement of the decay width by the PrimEx collaboration $\Gamma(\pi^0 \rightarrow \gamma\gamma) = (7.82 \pm 0.22) \text{ eV}$ [63]. We will take the corresponding precision of 1.4% for the form factor at vanishing momenta as conservative estimate on the normalization. An improvement from PrimEx-II is expected soon at the level of 0.7% for the form factor [64]. There are also plans to measure this decay at KLOE-2 with 0.5% statistical precision for

the normalization of the form factor [58]. Note that at the level of 1 – 2%, quark mass corrections and radiative corrections to the decay width need to be considered in order to compare theory [65] and experiment.

Another important experimental information is the slope of the form factor at the origin. Following Ref. [34], one defines⁷

$$b_{\pi^0} = \frac{1}{\mathcal{F}_{\pi^0\gamma^*\gamma^*}(0,0)} \left. \frac{d\mathcal{F}_{\pi^0\gamma^*\gamma^*}(q^2,0)}{dq^2} \right|_{q^2=0}. \quad (28)$$

The PDG [4] uses essentially the determination of the slope by CELLO [66] as their average $b_{\pi^0} = (1.76 \pm 0.22) \text{ GeV}^{-2}$, with a 12.5% precision (assuming that the systematic error is of the same size as the statistical error as stated in Ref. [66]). The CELLO collaboration was the first to measure the single-virtual form factor $\mathcal{F}_{\pi^0\gamma^*\gamma^*}(-Q^2, 0)$ for spacelike momenta in the momentum range 0.7 – 1.6 GeV in the process $e^+e^- \rightarrow e^+e^-\gamma^*\gamma^* \rightarrow e^+e^-\pi^0$. CELLO determines the slope of the form factor using a simple VMD ansatz with vector meson mass $\Lambda_{\pi^0} = (748 \pm 42) \text{ MeV}$ to fit the data and evaluates the slope at zero momentum from the fitted function as $b_{\pi^0} = 1/\Lambda_{\pi^0}^2$. As pointed out in Ref. [52], this large extrapolation from 0.7 GeV to the origin might induce a model dependence or bias that is not covered by the uncertainty from the fit to the data at higher energies. In Ref. [39] it was argued, based on Padé approximants to form factor measurements in the spacelike region by CELLO, CLEO [67] and BABAR [68], that there might be a 45% systematic uncertainty in the slope from the modelling and the large extrapolation. From a sequence of Padé approximants, Ref. [39] obtained the result $b_{\pi^0}[\text{Padé}] = (1.78 \pm 0.12) \text{ GeV}^{-2}$ with 6.9% precision. Other experimental determinations of the slope in the timelike region from the single Dalitz decay $\pi^0 \rightarrow e^+e^-\gamma$ in Ref. [69], published around the same time as CELLO and used in the PDG average, yield mostly similar central values, close to the CELLO result and the VMD prediction $b_{\pi^0}[\text{VMD}] = 1/M_\rho^2 = 1.66 \text{ GeV}^{-2}$, but with uncertainties of 100% or more (one experiment even obtained a negative central value). Note that a proper treatment of radiative corrections needs to be done in order to extract information on the form factor or the branching ratio $\text{BR}(\pi^0 \rightarrow e^+e^-\gamma)$ from the data, as discussed in Ref. [70].

The single-virtual form factor $\mathcal{F}_{\pi^0\gamma^*\gamma^*}(-Q^2, 0)$ for spacelike momenta has been measured by a series of experiments. The CELLO [66] measurement was done in the momentum range $0.7 \leq Q \leq 1.6 \text{ GeV}$ ($0.5 \leq Q^2 \leq 2.7 \text{ GeV}^2$). It has a precision of about 8 – 9% in the two bins from 0.7 – 1 GeV. Between 1 – 1.4 GeV, the precision is about 11 – 12% and for the highest bin 20%. Later, CLEO [67] measured the form factor in the region $1.2 \leq Q \leq 3 \text{ GeV}$ ($1.5 \leq Q^2 \leq 9 \text{ GeV}^2$). Between 1.2 – 1.5 GeV the precision is about 6 – 7%, between 1.5 – 2 GeV about 8 – 11% and above 2 GeV the uncertainty increases gradually to 15%. At higher energies, $2 \leq Q \leq 6.3 \text{ GeV}$ ($4 \leq Q^2 \leq 40 \text{ GeV}^2$), there are measurements of the form factor available from BABAR [68] and Belle [71]. Between 2 – 3 GeV the precision of BABAR is about 3 – 4%. For Belle, the form factor

⁷The PDG [4] parametrizes the form factor in conversion or Dalitz decays for small momenta in the linearized form $\mathcal{F}_{\pi^0\gamma^*\gamma^*}(q^2, 0) = \mathcal{F}_{\pi^0\gamma^*\gamma^*}(0, 0) (1 + a_{\pi^0} q^2/m_{\pi^0}^2)$, therefore $b_{\pi^0} = a_{\pi^0}/m_{\pi^0}^2$.

measurements in the two lowest bins with $2 \leq Q \leq 2.4$ GeV have errors of 16% and 13%, respectively. The error for the three next bins with $2.4 \leq Q \leq 3$ GeV then drops to 5 – 6%. There is a disagreement between the data of BABAR and Belle above about 3 GeV, with the BABAR data for the form factor not showing the $1/Q^2$ behavior expected from QCD [72]. While this puzzle needs to be clarified, the form factor data above 3 GeV is not very relevant for the muon $g - 2$, as already discussed in Ref. [73]. This can be seen from the plots of the weight functions in Fig. 2 and the results in Table 5.

An analysis is ongoing by BESIII [74] to measure the form factor in the region $0.5 \leq Q \leq 1.8$ GeV ($0.3 \leq Q^2 \leq 3.1$ GeV²) with a precision of 5 – 10%. Finally, according to the simulations performed in Ref. [58], KLOE-2 should be able to measure the form factor with 6% statistical precision at even lower energies: $0.1 \leq Q \leq 0.3$ GeV ($0.01 \leq Q^2 \leq 0.09$ GeV²).

In principle, one can obtain information about the single-virtual form factor $|\mathcal{F}_{\pi^0\gamma^*\gamma^*}(q^2, 0)|$ at small timelike momenta from the single Dalitz decay $\pi^0 \rightarrow \gamma^*\gamma \rightarrow e^+e^-\gamma$, see Ref. [69]. However, due to the small pion mass, the kinematical reach in $|q|$ is very small and form factor effects are not clearly visible. This explains the difficulty to extract for instance the slope parameter with a reasonable precision. At higher momenta, the form factor enters in the process $e^+e^- \rightarrow \gamma^* \rightarrow \pi^0\gamma$ and has been measured at SND and CMD-2 [75]. Of course, one cannot simply translate the form factor values $|\mathcal{F}_{\eta\gamma^*\gamma^*}(q^2, 0)|$ measured at timelike momenta q^2 into the spacelike region Q^2 . A proper analytical continuation needs to be performed, preferably without introducing too much model dependence.

Finally, recently a dispersion relation has been proposed in Ref. [44] to determine the single and double-virtual form factor. So far, only the single-virtual form factor has been evaluated in this dispersive framework. The dispersion relation yields, within uncertainties, a perfect description of the experimental data for $e^+e^- \rightarrow \pi^0\gamma$ from Ref. [75]. At small spacelike momenta, very small errors are obtained, e.g. for $Q = 0.25, 0.5, 1$ GeV, the uncertainties for $\mathcal{F}_{\pi^0\gamma^*\gamma^*}(-Q^2, 0)$ are 0.24%, 0.9%, 3.8% [76]. Note that to these uncertainties an error of about 1.4% for the normalization at $Q^2 = 0$ has to be added in quadrature. The normalization error might go down further soon, thanks to PrimEx-II [64]. The dispersion relation predicts the slope with 2% precision: $b_\pi[\text{DR}] = (1.69 \pm 0.03) \text{ GeV}^{-2}$. This agrees quite well with the naive VMD estimate, but this might be a coincidence, see the discussion in Ref. [44].

Based on the current experimental situation and the progress expected in the next few years, we obtain the momentum dependent errors $\delta_{1,\pi^0}(Q)$ in different bins as shown in Table 6 in Section 6. Currently, no experimental data on the pion TFF is available below the point $Q = 0.7$ GeV from CELLO [66], except for the normalization from $\Gamma(\pi^0 \rightarrow \gamma\gamma)$ and estimates of the slope. BESIII [74] should publish their results down to 0.5 GeV soon and also KLOE-2 [58] might perform measurements for $0.1 \leq Q \leq 0.3$ GeV. For the lowest bin $0 \leq Q < 0.5$ GeV, we therefore assume an error, based on “extrapolating” the current data sets and the data that will be available in a few years. In the bin 0.5 – 1 GeV mostly the data from CELLO and future BESIII data lead to the assumed precision, while in the region 1 – 2 GeV these are data from CLEO [67] and future BESIII data. Finally,

for 2 – 3 GeV, the data from BABAR [68] are the most precise. If one uses the dispersion relation from Ref. [44] below 1 GeV and the current error on the normalization from the decay width, one obtains (conservatively) the uncertainties in the lowest two bins given in brackets in Table 6.

The second ingredient in Eqs. (11) and (12) is the double-virtual form factor $\mathcal{F}_{\pi^0\gamma^*\gamma^*}(-Q_1^2, -Q_2^2)$. Currently, there are no direct experimental measurements available for this form factor at spacelike momenta. From the double Dalitz decay $\pi^0 \rightarrow \gamma^*\gamma^* \rightarrow e^+e^-e^+e^-$ one can obtain the double off-shell form factor $|\mathcal{F}_{\pi^0\gamma^*\gamma^*}(q_1^2, q_2^2)|$ at small invariant momenta in the timelike region [77], but the results are inconclusive, even translating into a negative value for the slope of the form factor $b_{\pi^0} = (-2.2 \pm 2.2) \text{ GeV}^{-2}$ (with 100% uncertainty). There might again be some issues with potentially large radiative corrections with respect to the extraction of the form factor and its slope from the data, see Refs. [78, 62].

From processes in the timelike region like $\omega \rightarrow \pi^0\gamma^* \rightarrow \pi^0\ell^+\ell^-$ ($\ell = e, \mu$), $\phi \rightarrow \pi^0\gamma^* \rightarrow \pi^0\ell^+\ell^-$ and $e^+e^- \rightarrow \gamma^* \rightarrow \omega\pi^0$ there is information available for $|\mathcal{F}_{\pi^0\gamma^*\gamma^*}(m_V^2, q^2)|$, i.e. along certain lines in the two dimensional plane (q_1^2, q_2^2) [33]. Again, it is not so straightforward to use this information measured far in the timelike region to obtain the form factor with spacelike momenta.

There is also indirect information available on the double off-shell form factor $\mathcal{F}_{\pi^0\gamma^*\gamma^*}(q_1^2, q_2^2)$ from the loop-induced decay $\pi^0 \rightarrow e^+e^-$ [4, 79]. Without a form factor at the $\pi^0 - \gamma^* - \gamma^*$ -vertex, the loop integral in this decay is ultraviolet divergent. One therefore obtains short-distance constraints on the form factor $\mathcal{F}_{\pi^0\gamma^*\gamma^*}(-Q_1^2, -Q_2^2)$ in the spacelike region, see Ref. [54]. The connection between the pion (pseudoscalar) decay into a lepton pair and the pion (pseudoscalar) pole contribution to HLbL was already pointed out in Refs. [21, 51]. It was later taken up in Ref. [80] and problems to explain both processes simultaneously with the same model have been stressed. Again, there are potential issues with radiative corrections to extract the decay rate $\pi^0 \rightarrow e^+e^-$ from the measured data, see Ref. [81].

The decay $\pi^0 \rightarrow \gamma\gamma$ and the double-virtual form factor $\mathcal{F}_{\pi^0\gamma^*\gamma^*}(-Q_1^2, -Q_2^2)$ has also been studied in Lattice QCD [82, 83] for spacelike and timelike momenta. While at low momenta a description of the form factor by the VMD model seems to work, at higher spacelike momenta, i.e. above 0.5 – 1 GeV, deviations are seen, in particular the impact of excited states in the vector channel. For the pion decay width the result $\Gamma(\pi^0 \rightarrow \gamma\gamma) = 7.83(31)(49) \text{ eV}$ has been quoted in the most recent paper in Ref. [83], rather close to the experimental result from the PDG and PrimEx, but the precision of 7.4% is not yet competitive with the experimental uncertainty. The result is the extrapolation to the physical pion mass, however, only one lattice spacing has been used. The double-virtual form factor with off-shell momenta has only been studied in Refs. [82, 83] for unphysical pion masses ($M_\pi \geq 300 \text{ MeV}$), which lead to vector-meson masses of 1 GeV or more. Therefore more studies are needed for firm conclusions about the applicability and generalization of VMD.

Because of the lack of direct experimental measurements of the double-virtual form factor $\mathcal{F}_{\pi^0\gamma^*\gamma^*}(-Q_1^2, -Q_2^2)$, models have been used to describe the form factor in the

spacelike region and thus all current evaluations of $a_\mu^{\text{HLbL};\pi^0}$ are model dependent. Often the assumption is made that the form factor factorizes $\mathcal{F}_{\pi^0\gamma^*\gamma^*}(-Q_1^2, -Q_2^2) = f(Q_1^2) \times f(Q_2^2)$, like in the popular VMD model, but, as already mentioned, this factorization is not expected in QCD. With this assumption, the double-virtual form factor is then completely determined by the single-virtual form factor where a lot of experimental information is available, although not yet in the low-momentum region $Q \leq 0.7$ GeV, which is very important for the pion-pole contribution, as we have seen before. Nevertheless, at least for low momenta, the assumption of factorization might work well numerically. For instance, the LMD+V model, which does not factorize, and the VMD model differ for $Q_1 = Q_2 = 0.5$ GeV by only 3%.

Of course, it would be preferable to replace these model assumptions as much as possible by experimental data. In fact, it is planned to determine the double-virtual form factor at BESIII for momenta $0.5 \leq Q_{1,2} \leq 1.5$ GeV and a first analysis is already in progress [42], based on existing data. More data will be collected in the coming years. Maybe at very low momenta $Q_{1,2} \leq 0.5$ GeV also KLOE-2 could measure this double-virtual form factor and Belle 2 could maybe measure it at higher momenta $Q_{1,2} \geq 1$ GeV. It would be highly welcome, if some simulations and data analysis would be performed.

The dispersion relation derived in Ref. [44] allows to determine the double-virtual form factor, but has not yet been evaluated. This might allow to check the factorization property, although at momenta approaching 1 GeV, where the LMD+V and the VMD model differ already by 23%, it remains to be seen whether the dispersive approach will give reliable results. If factorization works below 1 GeV, the precision of the dispersive approach for the form factor could be $2 \times 4\% = 8\%$ (or better), see Table 6.

In view of the current absence of direct experimental information on the double-virtual form factor $\mathcal{F}_{\pi^0\gamma^*\gamma^*}(-Q_1^2, -Q_2^2)$, we use as estimate of the measurement errors $\delta_{2,\pi^0}(Q_1, Q_2)$ the results of a Monte Carlo simulation [42] for the BESIII detector using the LMD+V model in the EKHARA event generator [84] for the signal process $e^+e^- \rightarrow e^+e^-\gamma^*\gamma^* \rightarrow e^+e^-\pi^0$. The results for $\delta_{2,\pi^0}(Q_1, Q_2)$ in different momentum bins are shown in Fig. 6 in Section 6.

Since the number of MC events N_i in bin number i is proportional to the cross-section σ_i (in that bin) and since for the calculation of the cross-section the form factor enters squared, the statistical error on the form factor measurement is given according to Poisson statistics by

$$\sigma_i \sim \mathcal{F}_{\pi^0\gamma^*\gamma^*}^2 \Rightarrow \frac{\delta \mathcal{F}_{\pi^0\gamma^*\gamma^*}}{\mathcal{F}_{\pi^0\gamma^*\gamma^*}} = \frac{\sqrt{N_i}}{2N_i}. \quad (29)$$

To simplify the appearance of Fig. 6, we have rounded the number of events from the Monte Carlo simulation to integer values (similarly for the percentage errors) and symmetrized the entries off the diagonal. In total there are 605 events in the displayed momentum region.

In the lowest momentum bin $Q_{1,2} \leq 0.5$ GeV, there are no events in the simulation, because of the acceptance of the detector. When both $Q_{1,2}^2$ are small, both photons are almost real and the scattered electrons and positrons escape detection along the beam pipe. As a further assumption, we have therefore taken the average of the uncertainties

in the three neighboring bins as estimate for the error in that lowest bin. This “extrapolation” from the neighboring bins seems justified, since information along the two axis is (or will soon be) available and the value at the origin is known quite precisely from the decay width. Note that although the form factor for spacelike (Euclidian) momenta is rather smooth in the two models considered in this paper (and in other models as well), see Fig. 7 in Appendix B, it is far from being a constant and some nontrivial extrapolation is needed. For instance for $Q^2 = (0.5 \text{ GeV})^2$ we get for both the LMD+V and the VMD model $\mathcal{F}_{\pi^0\gamma^*\gamma^*}(-Q^2, 0)/\mathcal{F}_{\pi^0\gamma^*\gamma^*}(0, 0) = 0.7$ and $\mathcal{F}_{\pi^0\gamma^*\gamma^*}(-Q^2, -Q^2)/\mathcal{F}_{\pi^0\gamma^*\gamma^*}(0, 0) = 0.5$. Of course, a direct experimental measurement in that lowest bin would be helpful. In the meantime, the dispersive approach from Ref. [44] will hopefully give reliable results at these low momenta.

The Monte Carlo simulation [42] corresponds to a data sample with an integrated luminosity of 2.9 fb^{-1} , collected at BESIII at an energy of $\sqrt{s} = 3.773 \text{ GeV}$. This is approximately half of the data set collected at BESIII so far. We should point out that the simulation only included signal events without any decay of the π^0 and assumed 100% detection efficiency and acceptance. There is a large background from Bhabha events with additional radiated photons, which has to be removed by cuts or more sophisticated analysis techniques, like neural networks. Based on a first preliminary analysis of the actual BESIII data [42] with strong cuts to reduce the background, it seems possible that the number of events and the corresponding precision for $\mathcal{F}_{\pi^0\gamma^*\gamma^*}(-Q_1^2, -Q_2^2)$ shown in Fig. 6 could be achievable with the current data set plus a few more years of data taking at BESIII.

On the other hand, once experimental data will be available, e.g. event rates in the different momentum bins, there will still be the task to unfold the data to reconstruct the form factor $\mathcal{F}_{\pi^0\gamma^*\gamma^*}(-Q_1^2, -Q_2^2)$. This should be done without introducing too much model dependence, i.e. more sophisticated approaches are needed than what is done for the single-virtual form factor where often a simple VMD form factor is used as fitting function. As a first approximation, one could maybe even use a constant form factor in each momentum bin. In this sense the situation is somewhat different from the hadronic vacuum polarization contribution to the muon $g - 2$, where one only needs to insert the hadronic cross-section into the dispersion integral with a known kernel function and can then use a simple trapezoidal rule to perform the integral.

5.2 η transition form factor

For the η -meson, the following experimental information is available about the single-virtual form factor $\mathcal{F}_{\eta\gamma^*\gamma^*}(-Q^2, 0)$. From the PDG average [4] for the decay width $\Gamma(\eta \rightarrow \gamma\gamma) = (0.516 \pm 0.018) \text{ keV}$ one obtains a 1.7% precision on the form factor normalization. The error is driven by the recent measurement $\Gamma(\eta \rightarrow \gamma\gamma) = (0.520 \pm 0.024) \text{ keV}$ by the KLOE-2 collaboration [85], which gives a 2.3% precision for the form factor at vanishing momenta.

In contrast to the pion, the single Dalitz decay $\eta \rightarrow \ell^+\ell^-\gamma$, with $\ell = e, \mu$ now has enough phase-space, so that the slope and the form factor can be measured in the time-

like region. The slope of the form factor at zero momentum has been extracted with a precision of 9.1% from measurements of the form factor by NA60 [86]⁸ and by A2 [88]: $b_\eta[\text{NA60, A2}] = (1.95 \pm 0.18) \text{ GeV}^{-2}$. The NA60 collaboration measured the Dalitz decay $\eta \rightarrow \mu^+ \mu^- \gamma$ approximately in the range $220 \leq |q| \leq 480 \text{ MeV}$, whereas the A2 collaboration measured the decay $\eta \rightarrow e^+ e^- \gamma$ down to very small momenta, $45 \leq |q| \leq 450 \text{ MeV}$. As in earlier experiments, a VMD ansatz was fitted to the data and from this fit function the slope was calculated. In Ref. [89] it was argued, based on an analysis using Padé approximants for the form factor, that the modelling of the data with a simple VMD ansatz and the extrapolation to zero might induce an additional error on the slope of about 5% for experimental determinations in the timelike region. Combining various recent timelike and spacelike data, Ref. [89] obtained a 2% determination of the slope: $b_\eta[\text{Padé}] = (1.919 \pm 0.037) \text{ GeV}^{-2}$, improving on an earlier 11% determination based on spacelike data in Ref. [40]: $b_\eta[\text{Padé, spacelike}] = (2.00 \pm 0.22) \text{ GeV}^{-2}$.

The slope was also determined from measurements of the form factor $\mathcal{F}_{\eta\gamma^*\gamma^*}(-Q^2, 0)$ in the spacelike region. The CELLO collaboration [66] measured in the region $0.5 - 1.8 \text{ GeV}$ and the slope was extracted with about 21% precision (assuming, as for the pion, that the systematic error is of the same size as the statistical error). However, since a simple VMD ansatz was fitted to the data above 0.5 GeV , there could be some large bias and uncertainty from the extrapolation to zero momentum, as already discussed in the context of determinations of the slope of the form factor for the pion. In fact, the fitted vector meson mass $\Lambda_\eta[\text{CELLO}] = (839 \pm 63) \text{ MeV}$ differs quite substantially from the value $\Lambda_\eta[\text{NA60, A2}] = (716 \pm 33) \text{ MeV}$ obtained by NA60 and A2. Shortly before CELLO, the form factor in the spacelike region has also been measured by the TPC/2 γ collaboration [90] in the region $0.3 - 2.6 \text{ GeV}$. The fitted vector meson mass $\Lambda_\eta[\text{TPC/2}\gamma] = (700 \pm 80) \text{ MeV}$ is rather close to the value extracted in the timelike region. The TPC/2 γ collaboration did not evaluate the slope, their measurement would translate into a precision of 23% for the slope. The fit by the CLEO collaboration [67] of their form factor data in the spacelike region from $1.2 - 4.5 \text{ GeV}$ with a VMD model yielded an even better determination of the vector meson mass $\Lambda_\eta(\text{CLEO}) = (774 \pm 29) \text{ MeV}$. This would formally translate into an 8% determination of the slope, but the extrapolation to zero seems even more questionable than for CELLO and therefore CLEO did not quote a value for the slope. The value of Λ_η by CLEO differs by two standard deviations from the results by NA60 and A2. There is, however, no reason why the fitted values of Λ_η for large spacelike and small timelike momenta should be the same. Note that we used the value of Λ_η from the CLEO fit to fix the vector meson mass in our VMD model to obtain the result in Eq. (23).

The form factor $\mathcal{F}_{\eta\gamma^*\gamma^*}(-Q^2, 0)$ has been measured in the spacelike region for the first time by the TPC/2 γ collaboration [90] for $0.3 \leq Q \leq 2.6 \text{ GeV}$ ($0.1 \leq Q^2 \leq 7 \text{ GeV}^2$). Since the data points are not tabulated, the measurement precision is difficult to estimate from the logarithmic plot in their paper. The CELLO [66] collaboration measured the form factor for $0.5 \leq Q \leq 1.8 \text{ GeV}$ ($0.3 \leq Q^2 \leq 3.4 \text{ GeV}^2$). The precision for $0.5 \leq Q \leq$

⁸In the conference proceedings [87] by the NA60 collaboration a further analysis even claimed a precision of 3.7% for the slope.

0.9 GeV is 14% and for $0.9 \leq Q \leq 1.1$ GeV about 19%. In the two bins above 1.1 GeV, the precision is 23% and 18%, respectively. The CLEO collaboration [67] measured the form factor in the range $1.2 \leq Q \leq 4.5$ GeV ($1.5 \leq Q^2 \leq 20$ GeV²). For 1.2 – 1.6 GeV the best precision in some decay channels is about 8 – 9%, between 1.6 – 2 GeV about 8 – 10% and above 2 GeV about 10 – 14% (or even more than 20% in the highest bin in some decay channels). More recently, BABAR [91] measured the form at higher momenta, $2 \leq Q \leq 6.3$ GeV ($4 \leq Q^2 \leq 40$ GeV²). Between 2 – 3 GeV the precision is about 4 – 5%. There is also one earlier measurement by BABAR at very large timelike momenta $q^2 = 112$ GeV² [92], which is compatible with the results for large spacelike momenta.

It is difficult to extract the precision of the measurement of the transition form factor $|\mathcal{F}_{\eta\gamma^*\gamma^*}(q^2, 0)|$ in the timelike region by the NA60 collaboration from the logarithmic plot in Ref. [86]. The precision of the form factor measurements by the A2 collaboration [88] between 45 – 150 MeV is about 1.5 – 2%, between 150 – 300 MeV about 2 – 5%, between 300 – 400 MeV about 5 – 11% and above 400 MeV around 15 – 28%. In the region 220 – 400 MeV, the precision of NA60 is about the same as A2, while above 400 MeV, the precision of NA60 seems a bit better. As for the pion, one then needs to properly map the values measured in the timelike into the spacelike region via an analytical continuation, without introducing new model dependence.

In Ref. [45] a dispersion relation was proposed and evaluated for the single-virtual TFF $\mathcal{F}_{\eta\gamma^*\gamma^*}(q^2, 0)$. It yields a rather precise prediction for the form factor and agrees well with the most precise measurements by NA60 [86, 87] and A2 [88] up to 0.25 GeV² in the timelike region. A prediction for the slope with a precision of 11% was given in Ref. [45], but it was later pointed out in Ref. [46] that there are effects of the a_2 -tensor meson in the left-hand cut of the form factor, which shift the slope down by about 7%. A recent reanalysis [47] then leads to the result $b_\eta[\text{DR}] = 1.9^{+0.2}_{-0.1}$ GeV⁻², i.e. with about 11% precision, neglecting the tiny effects -0.04 GeV⁻² from the isoscalar contribution. This value is compatible with the experimental results by NA60 and A2 and with the recent analysis using Padé approximants [40, 89], but bigger than older theoretical estimates [93], using ChPT (1-loop with resonance saturation for the low-energy constants), VMD, quark-loop models and the Brodsky-Lepage interpolation formula for the TFF.

From these observations, we deduce the values for the measurement errors $\delta_{1,\eta}(Q)$ for the single-virtual TFF $\mathcal{F}_{\eta\gamma^*\gamma^*}(-Q^2, 0)$ shown in Table 6. We assume an error in the lowest bin, $0 \leq Q \leq 0.5$ GeV, as done already for the pion. There is one data point available from a measurement by the TPC/2 γ collaboration [90], with a bin starting at 0.3 GeV, but it is difficult to estimate the uncertainty. We hope that the information on the normalization, the slope at zero and the data in the timelike region can be used to obtain some reliable estimate in that low momentum region. In the bin $0.5 \leq Q \leq 1$ GeV there is data available from TPC/2 γ and from CELLO [66], but they are not very precise. It would be very helpful, if BESIII could measure the η -TFF in that region in the near future. In the bin 1 – 2 GeV there is data available from CLEO [67] with about the given precision and for 2 – 3 GeV the data by BABAR [91] are the most precise.

Concerning the double-virtual form factor $\mathcal{F}_{\eta\gamma^*\gamma^*}(-Q_1^2, -Q_2^2)$, there are no measure-

ments in the spacelike region yet. The branching ratio of the double Dalitz decay $\eta \rightarrow e^+e^-e^+e^-$ has been measured [94], but no attempt was made to extract the TFF in the timelike region. Again, there are some indirect constraints from the loop-induced decay $\eta \rightarrow \mu^+\mu^-$ [4, 80], see also the recent analysis in Ref. [95]. The dispersive approach was recently extended to the double-virtual TFF $\mathcal{F}_{\eta\gamma^*\gamma^*}(q_1^2, q_2^2)$ in Ref. [47]. Because of limited input data for the DR, it could not be evaluated for general momenta. It was shown, however, that for $q_1^2 \ll 1 \text{ GeV}^2$ and $1 \text{ GeV}^2 \leq q_2^2 \leq (4.5 \text{ GeV})^2$ the form factor is compatible with the factorization ansatz, if the effects of the a_2 meson are taken into account.

We therefore use again the results of the MC simulation [42] for BESIII, but now with the VMD model in EKHARA [84] and display the corresponding estimates for the errors $\delta_{2,\eta}(Q_1, Q_2)$ in Fig. 6. For this simulation, there are in total 345 events in the given momentum region.

5.3 η' transition form factor

For the η' meson, one has the following experimental information about the single-virtual TFF $\mathcal{F}_{\eta'\gamma^*\gamma^*}(-Q^2, 0)$. The PDG average [4] $\Gamma(\eta' \rightarrow \gamma\gamma) = (4.28 \pm 0.19) \text{ keV}$ leads to a 2.2% determination on the form factor normalization at zero momentum. As for π^0 and η , the uncertainty is driven mostly by one experiment, this time by the L3 collaboration [96]. Their value $\Gamma(\eta' \rightarrow \gamma\gamma) = (4.17 \pm 0.29) \text{ keV}$ leads to a 3.5% precision for the form factor.

As for the η -meson, now the single Dalitz decay $\eta' \rightarrow \ell^+\ell^-\gamma, \ell = e, \mu$, has enough phase-space, so that the slope and the form factor can be measured. The slope of the form factor has been determined very recently with a precision of 11.7% from a measurement of the form factor $|\mathcal{F}_{\eta'\gamma^*\gamma^*}(q^2, 0)|$ in the timelike region by the BESIII collaboration [97]: $b_{\eta'}[\text{BESIII}] = (1.60 \pm 0.19) \text{ GeV}^{-2}$. The Dalitz decay $\eta' \rightarrow e^+e^-\gamma$ was measured in the momentum range $0 \leq |q| \leq 0.8 \text{ GeV}$. If one uses a simple VMD ansatz as in Eq. (B12), a pole appears in that momentum region at the vector meson mass. Therefore a Breit-Wigner ansatz with a pole mass Λ and a width γ has to be fitted (or a sum of such terms with several vector mesons like ρ, ω, ϕ , see also Ref. [34]). The BESIII data was fitted with a single vector meson and from this fit function the vector meson mass $\Lambda_{\eta'}[\text{BESIII}] = 790 \pm 40 \text{ MeV}$ and the corresponding slope was calculated. Using instead for the bins below 0.5 GeV, i.e. below the ρ -pole, a VMD ansatz without a width parameter leads to a value for the vector meson mass and the slope which is consistent with the first method. Previously, the slope had only been determined from a measurement of the form factor $|\mathcal{F}_{\eta'\gamma^*\gamma^*}(q^2, 0)|$ of the decay $\eta' \rightarrow \mu^+\mu^-\gamma$ by the Lepton-G collaboration [98] in the timelike region $0.2 \leq |q| \leq 0.9 \text{ GeV}$ with a precision of about 24% as quoted in Ref. [34], corresponding to $\Lambda_{\eta'}[\text{Lepton-G}] = 770 \pm 90 \text{ MeV}$.

Again there are also determinations of the slope by measurements of the form factor $\mathcal{F}_{\eta'\gamma^*\gamma^*}(-Q^2, 0)$ in the spacelike region. The form factor was measured by the L3 collaboration [96] in the region $0.1 \leq Q \leq 3.2 \text{ GeV}$. The data were fitted with a VMD ansatz with $\Lambda_{\eta'}[\text{L3}] = (900 \pm 51) \text{ MeV}$, which differs significantly from the value obtained by BESIII. The L3 collaboration did not translate their result into a determination of the

slope, which would give a 11.3% precision. Although there are three data points by L3 at rather low momentum values (two of them below 0.5 GeV), there are also two data points with large momenta above 1 GeV, which might distort the fit and the result for $\Lambda_{\eta'}$. The CELLO collaboration [66] has measured the form factor in the spacelike region 0.5–4.5 GeV and a VMD fit yielded $\Lambda_{\eta'}[\text{CELLO}] = 794 \pm 44$ MeV, which is rather close to the value obtained by BESIII. This gives a 15.7% determination of the slope (assuming, as for the pion, that the systematic error is of the same size as the statistical error). Shortly before CELLO, the TPC/2 γ collaboration [90] measured the form factor at slightly lower spacelike momenta 0.3 – 2.6 GeV and obtained $\Lambda_{\eta'}[\text{TPC}/2\gamma] = 850 \pm 70$ MeV, i.e. a bit higher than CELLO, but with similar precision. The TPC/2 γ collaboration did not evaluate the slope. As for the pion and the η , the VMD fit of the data measured by the CLEO collaboration [67] in the spacelike region 1.2 – 5.5 GeV yields the most precise determination of the vector meson mass parameter $\Lambda_{\eta'}[\text{CLEO}] = 859 \pm 28$ MeV. This result deviates by about two standard deviations from the values obtained by BESIII in the timelike region and by CELLO in the spacelike region. Again, because of the large extrapolation to zero momentum, CLEO did not quote a result for the slope. Formally, their result would be a determination of the slope with 6.6% precision. Note that we used the value of $\Lambda_{\eta'}$ from the CLEO fit to fix the vector meson mass in our VMD model to obtain the result in Eq. (24).

The form factor $\mathcal{F}_{\eta'\gamma^*\gamma^*}(-Q^2, 0)$ has been measured in the spacelike region for the first time by the PLUTO collaboration [99] for $0.4 \leq Q \leq 1.0$ GeV ($0.2 \leq Q^2 \leq 1$ GeV²). For the lowest bin 0.4 – 0.6 GeV the precision was about 20%, for the two higher bins only about 40%. Then there was the measurement by the TPC/2 γ collaboration [90] in the region $0.3 \leq Q \leq 2.6$ GeV ($0.1 \leq Q^2 \leq 7$ GeV²). The measurement precision is difficult to estimate from the logarithmic plot in their paper. The CELLO [66] collaboration measured the form factor for $0.5 \leq Q \leq 4.5$ GeV ($0.3 \leq Q^2 \leq 20$ GeV²). The precision for $0.5 \leq Q \leq 0.9$ GeV is about 11% and for $0.9 \leq Q \leq 1.1$ GeV about 13%. In the two bins 1.1 – 1.8 GeV, the precision is 14% and 17%, respectively, and above 1.8 GeV it is 30%. The CLEO collaboration [67] measured the form factor in the range $1.2 \leq Q \leq 4.5$ GeV ($1.5 \leq Q^2 \leq 30$ GeV²). For 1.2 – 1.6 GeV the best precision in some decay channels is about 7%, between 1.6 – 2 GeV about 8% and above 2 GeV about 8 – 12% (or much more in some decay channels). The L3 collaboration [96] measured the form factor in the region $0.1 \leq Q \leq 3.2$ GeV ($0.01 \leq Q^2 \leq 10$ GeV²). There are three untagged measurement points in the bins (0.1 – 0.4), (0.4 – 0.5), (0.5 – 0.9) GeV with precisions of 5%, 8%, 11%. The two bins with tagged events from 1.2 – 3.2 GeV have a precision of about 15%. More recently, BABAR [91] measured the form at higher momenta, $2 \leq Q \leq 6.3$ GeV ($4 \leq Q^2 \leq 40$ GeV²). Between 2 – 3 GeV the precision is about 4%. The measurement by BABAR at very large timelike momenta $q^2 = 112$ GeV² [92] is compatible with the results for large spacelike momenta.

The precision of the measurement of the form factor $|\mathcal{F}_{\eta'\gamma^*\gamma^*}(q^2, 0)|$ in the timelike region by BESIII [97] is about 2.8% in the lowest bin $|q| \leq 0.1$ GeV. For 0.1 – 0.3 GeV it is about 7% and for 0.3 – 0.5 GeV it is 11%. Just below the peak region 0.5 – 0.8 GeV it is about 14%. Since for the Lepton-G experiment [98] there is only a logarithmic plot

available in Ref. [34], it is not really possible to give an estimate on the precision. Again, one needs to perform an analytical continuation to obtain the form factor $\mathcal{F}_{\eta'\gamma^*\gamma^*}(-Q^2, 0)$ in the spacelike region.

The dispersion relation for the single-virtual η -TFF proposed in Ref. [45] can also be used for the η' -meson, under the additional assumption that the slopes of the pion spectra in $\eta \rightarrow \pi\pi\gamma$ and $\eta' \rightarrow \pi\pi\gamma$ are identical. This then yields $b_{\eta'}[\text{DR}] = 1.53^{+0.15}_{-0.08} \text{ GeV}^{-2}$ with about 10% precision. As can be seen from the erratum of Ref. [45], the assumption of an identical slope in the spectral shape is compatible with the data, but it might not be fulfilled completely. Furthermore, as pointed out in Ref. [46], there could be the effect of the a_2 -tensor meson in the left-hand cut of the form factor, which could be larger than for the η -TFF. Therefore, this dispersive evaluation of the slope needs to be scrutinized further, when more precise data become available in the future. The value for the slope itself agrees well with the new result by BESIII [97]. A recent determination of the slope using Padé approximants to spacelike and timelike TFF data yields a somewhat smaller central value: $b_{\eta'}[\text{Padé}] = (1.43 \pm 0.04) \text{ GeV}^{-2}$ [100] with about 3% precision, improving considerably on an earlier estimate that used only spacelike data: $b_{\eta'}[\text{Padé}; \text{spacelike}] = (1.42 \pm 0.18) \text{ GeV}^{-2}$ [40]. Older estimates based on ChPT, VMD and quark-loop models give here similar results [93].

From all these experimental results, we obtain the values for the measurement errors $\delta_{1,\eta'}(Q)$ for the single-virtual TFF $\mathcal{F}_{\eta'\gamma^*\gamma^*}(-Q^2, 0)$ shown in Table 6. For the η' -meson the experimental situation is a bit better than for π^0 and η , since there are in principle quite precise data available by the L3 collaboration [96] for $0.1 \leq Q \leq 0.5 \text{ GeV}$. Since these measurements of the form factor are based on untagged events, it would be good to have a cross check by some other experiment with lepton tagging in the future, like BESIII. In the bin $0.5 \leq Q \leq 1 \text{ GeV}$ there are measurements with similar precision available from L3 and CELLO [66]. Again, more precise data in this region from BESIII or Belle-2 would be very useful. In the bin $1 - 2 \text{ GeV}$ there are measurements with the given precision from CLEO [67] and for $2 - 3 \text{ GeV}$ the data of BABAR [91] have the precision listed in Table 6.

There are no measurements of the double-virtual form factor $\mathcal{F}_{\eta'\gamma^*\gamma^*}(-Q_1^2, -Q_2^2)$, neither in the spacelike nor the timelike region. According to Ref. [4] there are not even measurements of the corresponding branching ratios of the double Dalitz decays $\eta' \rightarrow \ell^+\ell^-\ell^+\ell^-$, $\ell = e, \mu$. Furthermore, there is only an upper bound on the branching ratio of the loop-induced decay $\eta' \rightarrow e^+e^-$ [4], see also the discussion in Ref. [95]. For the errors $\delta_{2,\eta'}(Q_1, Q_2)$ we use therefore again the results of the MC simulation [42] for BESIII with the VMD model in EKHARA [84] and display them in Fig. 6. There are 902 events in the given momentum region.

6 Impact of form factor uncertainties on $a_\mu^{\text{HLbL};\text{P}}$

Based on the discussion in the previous Section, we summarize in Table 6 the precision $\delta_{1,\text{P}}(Q)$ that is currently reached, or should soon be available, for the single-virtual TFF

$\mathcal{F}_{P\gamma^*\gamma^*}(-Q^2, 0)$ for all three light pseudoscalars. In Fig. 6 we show the estimated precision $\delta_{2,P}(Q_1, Q_2)$ for the double-virtual form factor $\mathcal{F}_{P\gamma^*\gamma^*}(-Q_1^2, -Q_2^2)$ based on the MC simulation for BESIII [42].

Table 6: Relative error $\delta_{1,P}(Q)$ on the form factor $\mathcal{F}_{P\gamma^*\gamma^*}(-Q^2, 0)$ for $P = \pi^0, \eta, \eta'$ in different momentum regions. The errors for $\delta_{1,\pi^0}(Q)$ and $\delta_{1,\eta}(Q)$ below 0.5 GeV are based on assumptions, see discussions in the text. In brackets for π^0 the uncertainties with a dispersion relation for the transition form factor.

Region [GeV]	$\delta_{1,\pi^0}(Q)$	$\delta_{1,\eta}(Q)$	$\delta_{1,\eta'}(Q)$
$0 \leq Q < 0.5$	5% [2%]	10%	6%
$0.5 \leq Q < 1$	7% [4%]	15%	11%
$1 \leq Q < 2$	8%	8%	7%
$2 \leq Q$	4%	4%	4%

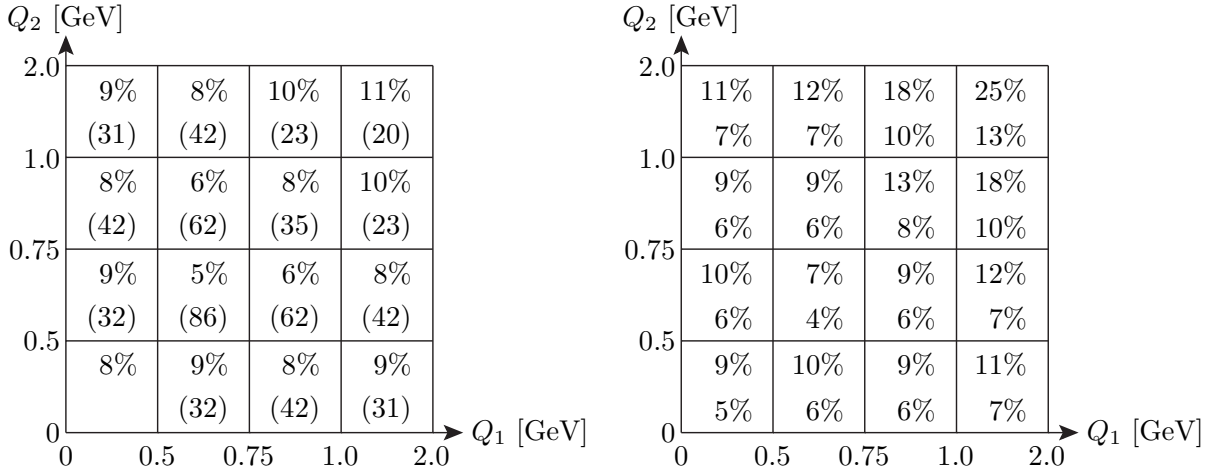


Figure 6: Left panel: Assumed relative error $\delta_{2,\pi^0}(Q_1, Q_2)$ of the pion TFF $\mathcal{F}_{\pi^0\gamma^*\gamma^*}(-Q_1^2, -Q_2^2)$ in different momentum bins. Note the unequal bin sizes. In brackets the number of MC events N_i in each bin according to the simulation with the LMD+V model for BESIII. In total, there are 605 events. For the lowest bin, $Q_{1,2} \leq 0.5$ GeV, there are no events in the simulation due to the detector acceptance. In that bin, we assume as error the average of the three neighboring bins. For $Q_{1,2} \geq 2$ GeV, we take a constant error of 15%. Right panel: Assumed relative error $\delta_{2,P}(Q_1, Q_2)$ of the form factor $\mathcal{F}_{P\gamma^*\gamma^*}(-Q_1^2, -Q_2^2)$ for $P = \eta, \eta'$ in different momentum bins according to the MC simulations with the VMD form factor for η (top line) and η' (bottom line). The error in the lowest bin is obtained by averaging the neighboring bins. For $Q_{1,2} \geq 2$ GeV, we assume a constant error of 25% for η and 15% for η' .

Taking again the LMD+V and VMD models for illustration, the assumed momentum dependent errors from Table 6 and Fig. 6 impact the precision for the pseudoscalar-pole contributions to HLbL as follows

$$a_{\mu; \text{LMD+V}}^{\text{HLbL}; \pi^0} = 62.9_{-8.2}^{+8.9} \times 10^{-11} \quad \left(\begin{smallmatrix} +14.1\% \\ -13.1\% \end{smallmatrix} \right), \quad (30)$$

$$a_{\mu; \text{VMD}}^{\text{HLbL}; \pi^0} = 57.0_{-7.3}^{+7.8} \times 10^{-11} \quad \left(\begin{smallmatrix} +13.7\% \\ -12.7\% \end{smallmatrix} \right), \quad (31)$$

$$a_{\mu; \text{VMD}}^{\text{HLbL}; \eta} = 14.5_{-3.0}^{+3.4} \times 10^{-11} \quad \left(\begin{smallmatrix} +23.4\% \\ -20.8\% \end{smallmatrix} \right), \quad (32)$$

$$a_{\mu; \text{VMD}}^{\text{HLbL}; \eta'} = 12.5_{-1.7}^{+1.9} \times 10^{-11} \quad \left(\begin{smallmatrix} +15.1\% \\ -13.9\% \end{smallmatrix} \right). \quad (33)$$

While for the pion the absolute variations are different for the two models, as are the central values, the relative uncertainty for both models is around 14%. This will also be visible in the following more detailed analysis. We therefore expect that using other form factor models, and, eventually, using experimental data for the single- and double-virtual form factors, will not substantially change the following observations and conclusions. Of course, a more sophisticated error analysis will be needed, once experimental informations on the double-virtual form factor will become available, also taking into account correlations between data points in different bins.

More details have been collected in Table 7, which contains the results from Eqs. (30)-(33) in the first line. The impact of the uncertainties in different momentum regions, below and above 0.5 GeV, are shown in the lines 2 – 5 in the table and potential further improvements in the last five lines. Line 6 shows the impact of the use of the DR for the single-virtual TFF $\mathcal{F}_{\pi^0 \gamma^* \gamma^*}(-Q^2, 0)$ for the pion in the two bins below 1 GeV, as indicated in Table 6. The lines 7 and 8 show the effect of an improvement of $\delta_{1,\eta}(Q)$ in the two bins below 1 GeV from 10%, 15% to 8%, 10% and of $\delta_{1,\eta'}(Q)$ from 6%, 11% to 5%, 8%. Such a precision is similar to what has already been achieved in the region 1 – 2 GeV and could for instance come from future measurements at BESIII. Line number 9 shows the precision on $a_{\mu}^{\text{HLbL}; \pi^0, \eta, \eta'}$ from an improvement in the lowest bin of $\delta_2(Q_1, Q_2)$ from 8%, 9%, 5% to 5%, 7%, 4%, i.e. what is obtained in the MC simulation for the second bin along the diagonal in Fig. 6. Finally, line 10 shows what would happen, if the second bins along the two axis in δ_2 would have the same precision as well, i.e. all four bins below 0.75 GeV would have the same precision as the second bin along the diagonal.

For the pion, the largest uncertainty of about 5% comes from the lowest bin $Q_{1,2} \leq 0.5$ GeV in the (Q_1, Q_2) -plane for δ_2 in Fig. 6 (fourth line in the table). Some improvement could be achieved, if the error in that lowest bin and the neighboring bins ($Q_{1,2} \leq 0.75$ GeV) could be reduced, to a total error of about 12%, see the lines 9 and 10 in Table 7. The second largest uncertainty of 4.4% for the pion stems from the lowest bin $Q < 0.5$ GeV in δ_1 (second line in the table). Here the use of a dispersion relation for the single-virtual form factor $\mathcal{F}_{\pi^0 \gamma^* \gamma^*}(-Q^2, 0)$ for $Q < 1$ GeV (see values in brackets in Table 6) could bring the total error of 14% down to 11%, see the sixth line. As seen from the plots of the weight functions and the relative contribution to the total from different momentum regions in Fig. 5, for the pion more precise data for the single- and double-virtual form factor in the region below 0.5 GeV would be very important to reduce the error for the pion-pole contribution to HLbL.

Table 7: Impact of assumed measurement errors $\delta_{1,P}(Q)$ and $\delta_{2,P}(Q_1, Q_2)$ in the form factors $\mathcal{F}_{P\gamma^*\gamma^*}(-Q^2, 0)$ and $\mathcal{F}_{P\gamma^*\gamma^*}(-Q_1^2, -Q_2^2)$ on the relative precision of the pseudoscalar-pole contributions (first line). Lines 2 – 5 show the effects of uncertainties in different momentum regions below and above 0.5 GeV. Lines 6 – 10 show the impact of potential improvements of some of the assumed errors.

$\frac{\delta a_{\mu; \text{LMD}+V}^{\text{HLbL}; \pi^0}}{a_{\mu; \text{LMD}+V}^{\text{HLbL}; \pi^0}}$	$\frac{\delta a_{\mu; \text{VMD}}^{\text{HLbL}; \pi^0}}{a_{\mu; \text{VMD}}^{\text{HLbL}; \pi^0}}$	$\frac{\delta a_{\mu; \text{VMD}}^{\text{HLbL}; \eta}}{a_{\mu; \text{VMD}}^{\text{HLbL}; \eta}}$	$\frac{\delta a_{\mu; \text{VMD}}^{\text{HLbL}; \eta'}}{a_{\mu; \text{VMD}}^{\text{HLbL}; \eta'}}$	Comment
+14.1% -13.1%	+13.7% -12.7%	+23.4% -20.8%	+15.1% -13.9%	Given δ_1, δ_2
+4.3% -4.2%	+4.4% -4.3%	+6.9% -6.8%	+3.4% -3.3%	Bin $Q < 0.5$ GeV in δ_1 as given, rest: $\delta_{1,2} = 0$
+1.1% -1.0%	+1.0% -0.9%	+4.4% -4.3%	+4.5% -4.4%	Bins $Q \geq 0.5$ GeV in δ_1 as given, rest: $\delta_{1,2} = 0$
+4.5% -4.4%	+4.9% -4.8%	+4.0% -4.0%	+1.7% -1.7%	Bin $Q_{1,2} < 0.5$ GeV in δ_2 as given, rest: $\delta_{1,2} = 0$
+3.9% -3.8%	+3.2% -3.1%	+7.0% -6.8%	+5.1% -5.0%	Bins $Q_{1,2} \geq 0.5$ GeV in δ_2 as given, rest: $\delta_{1,2} = 0$
+10.9% -10.5%	+10.6% -10.1%	—	—	Given δ_1, δ_2 , lowest two bins in δ_{1, π^0} : 2%, 4%
—	—	+20.4% -18.5%	—	Given δ_1, δ_2 , lowest two bins in $\delta_{1, \eta}$: 8%, 10%
—	—	—	+13.4% -12.5%	Given δ_1, δ_2 , lowest two bins in $\delta_{1, \eta'}$: 5%, 8%
+12.4% -11.6%	+11.8% -11.0%	+22.4% -20.0%	+14.8% -13.6%	π^0, η, η' : given δ_1, δ_2 , lowest bin δ_2 : 5%, 7%, 4%
+12.0% -11.2%	+11.4% -10.6%	+21.9% -19.6%	+14.4% -13.4%	In addition, bins in δ_2 close to lowest: 5%, 7%, 4%

For the η meson, the largest uncertainties of 7% originate from the region of δ_2 above 0.5 GeV (5th line) and from the lowest bin in δ_1 (2nd line). For the η' , the largest uncertainty of 5% comes again from the region of δ_2 above 0.5 GeV (5th line). The second largest uncertainty of 4.5% comes from the bins in δ_1 above 0.5 GeV (3rd line). For η and η' the errors go down to 20% and 13%, if the uncertainty in the two lowest bins in δ_1 could be reduced, see lines 7 and 8 in Table 7. There is only a small reduction of the uncertainty by one percentage point, if the errors in the lowest few bins of δ_2 with $Q_{1,2} \leq 0.75$ GeV could be reduced further, see lines 9 and 10. This is not unexpected, since for the η and η' that very-low momentum region is not as important as for the π^0 , see Fig. 5. Here, more precise data on the single- and double-virtual form factor in some intermediate region 0.5 – 1.5 GeV would be very important to reduce the uncertainty of the η - and η' -pole contributions to HLbL.

The size of the uncertainties can be understood approximately as follows. If the errors would be independent of the momenta and small, so that it is sufficient to take only the terms linear in $\delta_{1,P}$ and $\delta_{2,P}$, one would expect the following uncertainty for the pseudoscalar-pole contribution

$$\delta a_{\mu}^{\text{HLbL}; P} \approx (\delta_{1,P} + \delta_{2,P}) a_{\mu}^{\text{HLbL}; P}. \quad (34)$$

While the situation is more complicated with the given momentum dependent errors, one can observe the following for the impact of the uncertainties in the region below 0.5 GeV. We only discuss the case of the pion with the LMD+V form factor. The analysis is similar for the pion with the VMD form factor and for η and η' with the VMD form factor. For the LMD+V model, the region $Q_{1,2} < 0.5$ GeV yields 59% of the total result, see Table 5. Therefore, the effect of the lowest bin of δ_{2,π^0} in the (Q_1, Q_2) -plane with an assumed uncertainty of 8% (see Fig. 6) translates with $\delta_{1,\pi^0} = 0$ in Eq. (34) to about $8\% \times 0.59 \approx 4.7\%$ error in $a_\mu^{\text{HLbL};\pi^0}$. This agrees quite well with the 4.5% in line 4 of Table 7. In doing so we neglected, however, in the numerically dominating contribution in Eq. (11), which involves the weight function w_1 and the double-virtual form factor $\mathcal{F}_{\pi^0\gamma^*\gamma^*}(-Q_1^2, -(Q_1 + Q_2)^2)$, the momentum dependence in $\delta_{2,\pi^0}(|Q_1|, |Q_1 + Q_2|)$ with $|Q_1 + Q_2| = \sqrt{Q_1^2 + 2Q_1Q_2\tau + Q_2^2}$, see Eq. (27). This momentum dependence in δ_{2,π^0} leads to an upper cutoff of 0.5 GeV on Q_1 and to a cutoff on Q_2 , which varies between 0 – 1 GeV as a function of Q_1 and τ . However, as can be seen from Fig. 5, summing up all the bins with $Q_1 < 0.5$ GeV and $Q_2 < 1$ GeV adds at most a few percent to the 59%.

On the other hand, looking at the impact of a non-zero $\delta_{1,\pi^0}(Q)$ for $Q < 0.5$ GeV in line 2 in Table 7 (with $\delta_{2,\pi^0} = 0$ in Eq. (34)), one has to take into account that in Eq. (11) the single-virtual form factor $\mathcal{F}_{\pi^0\gamma^*\gamma^*}(-Q_2^2, 0)$ enters. Therefore the corresponding non-zero $\delta_{1,\pi^0}(Q_2)$ restricts only the integration region $Q_2 < 0.5$ GeV, while Q_1 runs up to infinity. This amounts to summing up the individual bins in Fig. 5 in the direction of Q_1 with $Q_2 < 0.5$ GeV, i.e. the lowest two bins in the Q_2 -direction. This summation yields about 85% of the total. With a precision of 5% in δ_{1,π^0} this gives $85\% \times 0.05 \approx 4.2\%$, to be compared with 4.3% in Table 7.

7 Conclusions

Recently, a dispersive approach to HLbL in the muon $g - 2$ has been proposed in Refs. [31, 32], which connects the presumably numerically dominant contributions from the light pseudoscalars ($P = \pi^0, \eta, \eta'$) and the two-pion intermediate states to, in principle, measurable quantities, like the single- and double-virtual pseudoscalar transition form factor $\mathcal{F}_{P\gamma^*\gamma^*}(-Q_1^2, -Q_2^2)$ and the scattering of two off-shell photons into two pions.

In this paper we studied in detail the pseudoscalar-pole contribution to HLbL in this dispersive framework. The three-dimensional integral representation for $a_\mu^{\text{HLbL};P}$ from Ref. [2], shown in Eqs. (11) and (12), allows one to separate the generic kinematics, described by model-independent weight functions $w_{1,2}(Q_1, Q_2, \tau)$, from the double-virtual transition form factors $\mathcal{F}_{P\gamma^*\gamma^*}(-Q_1^2, -Q_2^2)$, which can, in principle, be measured. From the weight functions one can already identify which are the most important momentum regions in the pseudoscalar-pole contribution to HLbL. However, the weight-function w_1 has a slowly decreasing ridge and the corresponding integral for HLbL diverges without form factors. We therefore used two simple form factor models (LMD+V, VMD) to evaluate $a_\mu^{\text{HLbL};P}$. From this we deduced that the relevant momentum region for π^0 is below about 1 GeV, irrespective of which of the two models is used. For η and η' , we only

used a simple VMD model and showed that the region below about 1.5 GeV gives the bulk of the result. However, since the double-virtual VMD form factor falls off too fast at high momenta compared to the predictions of the OPE, it might be that the momentum region 1.5–2.5 GeV is cut off too much. It would therefore be very useful, if experimental data on the double-virtual form factor, e.g. from planned measurements at BESIII, could reduce this model dependence.

If the assumed measurement errors $\delta_{1,P}(Q)$ in Table 6 and $\delta_{2,P}(Q_1, Q_2)$ in Fig. 6 on the single- and double-virtual TFF can be achieved in the coming years, one could obtain the following, largely data driven, uncertainties for the pseudoscalar-pole contributions to HLbL (see Eqs. (30)-(33) and Table 7)

$$\frac{\delta a_{\mu}^{\text{HLbL};\pi^0}}{a_{\mu}^{\text{HLbL};\pi^0}} = 14\% \quad [11\%], \quad (35)$$

$$\frac{\delta a_{\mu}^{\text{HLbL};\eta}}{a_{\mu}^{\text{HLbL};\eta}} = 23\%, \quad (36)$$

$$\frac{\delta a_{\mu}^{\text{HLbL};\eta'}}{a_{\mu}^{\text{HLbL};\eta'}} = 15\%. \quad (37)$$

The result in bracket for the pion in Eq. (35) uses the DR [44] for the single-virtual TFF $\mathcal{F}_{\pi^0\gamma^*\gamma^*}(-Q^2, 0)$ below 1 GeV. Compared to the range of estimates in the literature in Eqs. (9) and (10) this would definitely be some progress, as it would be largely based on experimental input data only. More work is needed, however, to reach a precision of 10% for all three contributions which is envisioned in the data-driven approach to HLbL [31, 32]. We have shown in Table 7, what would be the impact of further potential improvements in the measurement precision of the single-virtual TFF below 1 GeV and the double-virtual form factor below about 0.75 GeV.

One should keep in mind that the MC simulation from which the estimates for $\delta_{2,P}$ are derived, only considered the signal process and no backgrounds. On the other hand, since the simulation was based on about half of the data already collected at BESIII, it seems not unreasonable that the assumed precision could be reached with the full, almost doubled, data set in a few years, when appropriate cuts are imposed or more sophisticated analysis tools are used [42]. It remains to be seen, how the unfolding of event rates can be done to reconstruct the form factors, without introducing too much model dependence. Once this is achieved, a much more refined analysis can be performed, combining all existing data for the single- and double-virtual TFF, also taking into account correlations. One can then also combine this with the dispersive framework for the TFF themselves [44, 45, 46, 47].

We hope that our analysis of the relevant momentum regions in HLbL will be a useful guide for the experimental collaborations to look in more details at the various processes where the single- and double-virtual form factors can be measured. For instance, measurements of the double-virtual form factors, e.g. by KLOE-2 for π^0 in the low-momentum region $Q \leq 0.5$ GeV, where BESIII cannot detect any events, or by Belle 2 for η, η' for higher momenta, 1 – 1.5 GeV, would be very helpful.

We close by noting that similar three-dimensional integral representations with corresponding weight functions have been derived for the scalar-exchange contribution to HLbL in Ref. [38] and for all contributions to HLbL in Refs. [101, 31]. They can be analyzed along the same lines as shown here for w_1 and w_2 for the pseudoscalars to identify the relevant momentum regions in a model-independent way. This in turn can then help to plan future measurement, e.g. for $\gamma^*\gamma^* \rightarrow \pi^+\pi^-, \pi^0\pi^0$, which is needed as input for the dispersive framework [31, 32]. In this way, a concerted effort of theory and experiment can hopefully reduce and better control the uncertainty in the HLbL contribution to the muon $g-2$, so that one can fully profit from the upcoming future experiments at Fermilab and J-PARC [16].

Acknowledgments

I am grateful to Achim Denig, Christoph Redmer and Pascal Wasser for providing me with results of MC simulations for planned transition form factor measurements at BE-SIII and to Martin Hoferichter and Bastian Kubis for sharing information about the precision of the DR approach to the pion TFF. I thank them and Hans Bijnens, Gilberto Colangelo, Henryk Czyż, Simon Eidelman, Fred Jegerlehner, Marc Knecht, Marc Vanderhaeghen and Graziano Venanzoni for discussions and suggestions. This work was supported by Deutsche Forschungsgemeinschaft (DFG) through the Collaborative Research Center “The Low-Energy Frontier of the Standard Model” (SFB 1044).

A Weight functions in the integral representations for $a_\mu^{\text{HLbL};\pi^0}$

The kinematic functions in the two-loop integral for $a_\mu^{\text{HLbL};\pi^0}$ in Eqs. (7) and (8) have been evaluated in Ref. [21] and read as follows

$$\begin{aligned} \tilde{T}_1(q_1, q_2; p) = & (-64\pi^6) \left[\frac{16}{3} (p \cdot q_1) (p \cdot q_2) (q_1 \cdot q_2) - \frac{16}{3} (p \cdot q_2)^2 q_1^2 \right. \\ & - \frac{8}{3} (p \cdot q_1) (q_1 \cdot q_2) q_2^2 + 8(p \cdot q_2) q_1^2 q_2^2 - \frac{16}{3} (p \cdot q_2) (q_1 \cdot q_2)^2 \\ & \left. + \frac{16}{3} m_\mu^2 q_1^2 q_2^2 - \frac{16}{3} m_\mu^2 (q_1 \cdot q_2)^2 \right], \end{aligned} \quad (\text{A1})$$

$$\begin{aligned} \tilde{T}_2(q_1, q_2; p) = & (-64\pi^6) \left[\frac{16}{3} (p \cdot q_1) (p \cdot q_2) (q_1 \cdot q_2) - \frac{16}{3} (p \cdot q_1)^2 q_2^2 \right. \\ & + \frac{8}{3} (p \cdot q_1) (q_1 \cdot q_2) q_2^2 + \frac{8}{3} (p \cdot q_1) q_1^2 q_2^2 \\ & \left. + \frac{8}{3} m_\mu^2 q_1^2 q_2^2 - \frac{8}{3} m_\mu^2 (q_1 \cdot q_2)^2 \right]. \end{aligned} \quad (\text{A2})$$

Recall that the muon momentum is on-shell: $p^2 = m_\mu^2$.

The model-independent weight functions from the three-dimensional integral representation for $a_\mu^{\text{HLbL};\pi^0}$ in Eqs. (11) and (12) read [2]

$$w_1(Q_1, Q_2, \tau) = \left(-\frac{2\pi}{3}\right) \sqrt{1-\tau^2} \frac{Q_1^3 Q_2^3}{Q_2^2 + m_\pi^2} I_1(Q_1, Q_2, \tau), \quad (\text{A3})$$

$$w_2(Q_1, Q_2, \tau) = \left(-\frac{2\pi}{3}\right) \sqrt{1-\tau^2} \frac{Q_1^3 Q_2^3}{Q_3^2 + m_\pi^2} I_2(Q_1, Q_2, \tau), \quad (\text{A4})$$

with

$$\begin{aligned} I_1(Q_1, Q_2, \tau) = & X(Q_1, Q_2, \tau) \left(8 P_1 P_2 (Q_1 \cdot Q_2) - 2 P_1 P_3 (Q_2^4/m_\mu^2 - 2 Q_2^2) \right. \\ & - 2 P_1 (2 - Q_2^2/m_\mu^2 + 2 (Q_1 \cdot Q_2)/m_\mu^2) + 4 P_2 P_3 Q_1^2 \\ & - 4 P_2 - 2 P_3 (4 + Q_1^2/m_\mu^2 - 2 Q_2^2/m_\mu^2) + 2/m_\mu^2 \Big) \\ & - 2 P_1 P_2 (1 + (1 - R_{m1}) (Q_1 \cdot Q_2)/m_\mu^2) \\ & + P_1 P_3 (2 - (1 - R_{m1}) Q_2^2/m_\mu^2) + P_1 (1 - R_{m1})/m_\mu^2 \\ & + P_2 P_3 (2 + (1 - R_{m1})^2 (Q_1 \cdot Q_2)/m_\mu^2) + 3 P_3 (1 - R_{m1})/m_\mu^2, \quad (\text{A5}) \end{aligned}$$

and

$$\begin{aligned} I_2(Q_1, Q_2, \tau) = & X(Q_1, Q_2, \tau) \left(4 P_1 P_2 (Q_1 \cdot Q_2) + 2 P_1 P_3 Q_2^2 - 2 P_1 + 2 P_2 P_3 Q_1^2 \right. \\ & - 2 P_2 - 4 P_3 - 4/m_\mu^2 \Big) \\ & - 2 P_1 P_2 - 3 P_1 (1 - R_{m2})/(2m_\mu^2) - 3 P_2 (1 - R_{m1})/(2m_\mu^2) \\ & - P_3 (2 - R_{m1} - R_{m2})/(2m_\mu^2) \\ & + P_1 P_3 (2 + 3 (1 - R_{m2}) Q_2^2/(2m_\mu^2) + (1 - R_{m2})^2 (Q_1 \cdot Q_2)/(2m_\mu^2)) \\ & + P_2 P_3 (2 + 3 (1 - R_{m1}) Q_1^2/(2m_\mu^2) + (1 - R_{m1})^2 (Q_1 \cdot Q_2)/(2m_\mu^2)), \quad (\text{A6}) \end{aligned}$$

where⁹

$$Q_3^2 = (Q_1 + Q_2)^2 = Q_1^2 + 2Q_1 \cdot Q_2 + Q_2^2, \quad (\text{A7})$$

$$Q_1 \cdot Q_2 = Q_1 Q_2 \tau, \quad (\text{A8})$$

$$\tau = \cos \theta, \quad (\text{A9})$$

⁹Except in $Q_1 \cdot Q_2$, we always use the notation $Q_i \equiv |(Q_i)_\mu|, i = 1, 2$, for the length of the Euclidean four-momenta.

and we introduced the notation $P_1^2 = 1/Q_1^2$, $P_2^2 = 1/Q_2^2$, $P_3^2 = 1/Q_3^2$ for the photon propagators. Furthermore

$$X(Q_1, Q_2, \tau) = \frac{1}{Q_1 Q_2 x} \arctan \left(\frac{zx}{1 - z\tau} \right), \quad (\text{A10})$$

$$x = \sqrt{1 - \tau^2}, \quad (\text{A11})$$

$$z = \frac{Q_1 Q_2}{4m_\mu^2} (1 - R_{m1}) (1 - R_{m2}), \quad (\text{A12})$$

$$R_{mi} = \sqrt{1 + 4m_\mu^2/Q_i^2}, \quad i = 1, 2. \quad (\text{A13})$$

Note that $w_2(Q_1, Q_2, \tau)$ in Eq. (A4) and $I_2(Q_1, Q_2, \tau)$ in Eq. (A6) are symmetric under $Q_1 \leftrightarrow Q_2$.

For small momenta, these weight functions have the following behavior

$$\lim_{Q_1 \rightarrow 0} w_1(Q_1, Q_2, \tau) = \frac{16\pi}{3m_\mu^2} \frac{m_\mu Q_2 x^3 + (Q_2^2 - 2m_\mu^2)x^2 A(Q_2, \tau)}{Q_2^2 + m_\pi^2} Q_1^2 + \mathcal{O}(Q_1^3), \quad (\text{A14})$$

$$\lim_{Q_2 \rightarrow 0} w_1(Q_1, Q_2, \tau) = -\frac{32\pi}{3m_\pi^2} x^2 A(Q_1, \tau) Q_2^2 + \mathcal{O}(Q_2^3), \quad (\text{A15})$$

$$\lim_{Q \rightarrow 0} w_1(Q, Q, \tau) = -\frac{16\pi}{3m_\pi^2} (1 - \tau) \operatorname{arccot} \left[\frac{-1 + \tau}{x} \right] Q^2 + \mathcal{O}(Q^3), \quad (\text{A16})$$

$$\begin{aligned} \lim_{Q_1 \rightarrow 0} w_2(Q_1, Q_2, \tau) &= -\frac{4\pi}{3m_\mu^2} \frac{Q_2 x (2m_\mu - Q_2 \tau (1 - R_{m2})) + 2(Q_2^2 + 2m_\mu^2 x^2) A(Q_2, \tau)}{Q_2^2 + m_\pi^2} Q_1^2 \\ &+ \mathcal{O}(Q_1^3), \end{aligned} \quad (\text{A17})$$

$$\begin{aligned} \lim_{Q_2 \rightarrow 0} w_2(Q_1, Q_2, \tau) &= -\frac{4\pi}{3m_\mu^2} \frac{Q_1 x (2m_\mu - Q_1 \tau (1 - R_{m1})) + 2(Q_1^2 + 2m_\mu^2 x^2) A(Q_1, \tau)}{Q_1^2 + m_\pi^2} Q_2^2 \\ &+ \mathcal{O}(Q_2^3), \end{aligned} \quad (\text{A18})$$

$$\lim_{Q \rightarrow 0} w_2(Q, Q, \tau) = -\frac{8\pi}{3m_\pi^2} (1 - \tau) \operatorname{arccot} \left[\frac{-1 + \tau}{x} \right] Q^2 + \mathcal{O}(Q^3), \quad (\text{A19})$$

where we introduced the abbreviation

$$A(Q_i, \tau) = \arctan \left[\frac{Q_i x (1 - R_{mi})}{Q_i \tau (1 - R_{mi}) + 2m_\mu} \right], \quad i = 1, 2. \quad (\text{A20})$$

One observes that the weight functions $w_{1,2}(Q_1, Q_2, \tau)$ not only vanish for small momenta, but also the slopes along the two axis and along the diagonal $Q_1 = Q_2 = Q$ are zero

$$\left. \frac{\partial w_{1,2}(Q_1, Q_2, \tau)}{\partial Q_1} \right|_{Q_1=0} = \left. \frac{\partial w_{1,2}(Q_1, Q_2, \tau)}{\partial Q_2} \right|_{Q_2=0} = \left. \frac{\partial w_{1,2}(Q, Q, \tau)}{\partial Q} \right|_{Q=0} = 0. \quad (\text{A21})$$

On the other hand, for large momenta we get

$$\lim_{Q_1 \rightarrow \infty} w_1(Q_1, Q_2, \tau) = \frac{8\pi}{3m_\mu^2} \frac{Q_2^3 (Q_2^2 - R_{m2}(Q_2^2 - 2m_\mu^2))}{(Q_2^2 + m_\pi^2)} x^3 \frac{1}{Q_1} + \mathcal{O}\left(\frac{1}{Q_1^2}\right), \quad (\text{A22})$$

$$\lim_{Q_2 \rightarrow \infty} w_1(Q_1, Q_2, \tau) = -\frac{8\pi}{3m_\mu^2} Q_1^2 (2m_\mu^2 + Q_1^2(1 - R_{m1})) \tau x^3 \frac{1}{Q_2^2} + \mathcal{O}\left(\frac{1}{Q_2^3}\right), \quad (\text{A23})$$

$$\lim_{Q \rightarrow \infty} w_1(Q, Q, \tau) = \frac{8\pi m_\mu^2}{3} (3 - \tau)(1 - \tau) x \frac{1}{Q^2} + \mathcal{O}\left(\frac{1}{Q^4}\right), \quad (\text{A24})$$

$$\begin{aligned} \lim_{Q_1 \rightarrow \infty} w_2(Q_1, Q_2, \tau) &= -\frac{8\pi}{9m_\mu^2} Q_2^3 (m_\mu^2(3 - R_{m2}) + Q_2^2(1 - R_{m2})) x^3 \frac{1}{Q_1^3} \\ &\quad + \mathcal{O}\left(\frac{1}{Q_1^4}\right), \end{aligned} \quad (\text{A25})$$

$$\begin{aligned} \lim_{Q_2 \rightarrow \infty} w_2(Q_1, Q_2, \tau) &= -\frac{8\pi}{9m_\mu^2} Q_1^3 (m_\mu^2(3 - R_{m1}) + Q_1^2(1 - R_{m1})) x^3 \frac{1}{Q_2^3} \\ &\quad + \mathcal{O}\left(\frac{1}{Q_2^4}\right), \end{aligned} \quad (\text{A26})$$

$$\lim_{Q \rightarrow \infty} w_2(Q, Q, \tau) = \frac{4\pi m_\mu^4}{9} \frac{(2 - \tau)(1 - \tau)^{3/2}}{\sqrt{1 + \tau}} \frac{1}{Q^4} + \mathcal{O}\left(\frac{1}{Q^6}\right). \quad (\text{A27})$$

The slower fall off of $w_1(Q_1, Q_2, \tau)$ for large Q_1 in Eq. (A22), compared to the behavior for large Q_2 in Eq. (A23), leads to the ridge seen in Fig. 2 and, for a constant Wess-Zumino-Witten form factor, to the $\ln^2 \Lambda$ divergence for some momentum cutoff Λ . Of course, the symmetric function $w_2(Q_1, Q_2, \tau)$ cannot show such a behavior.

Finally, for $\tau \rightarrow \pm 1$, the weight functions behave as follows

$$\begin{aligned} \lim_{\tau \rightarrow 1} w_1(Q_1, Q_2, \tau) &= \frac{16\sqrt{2}\pi}{3m_\mu^2} \frac{(1 - R_{m1})Q_1^3 Q_2^3}{(Q_2^2 + m_\pi^2)(Q_1 + Q_2)^2 (4m_\mu^2 - Q_1 Q_2(1 - R_{m1})(1 - R_{m2}))} \\ &\quad \times [-4m_\mu^2 R_{m2} + (Q_2(1 - R_{m2})(Q_1(1 - R_{m1}) - 2Q_2))] (1 - \tau)^{3/2} \\ &\quad + \mathcal{O}((1 - \tau)^{5/2}), \end{aligned} \quad (\text{A28})$$

$$\lim_{\tau \rightarrow 1} w_1(Q, Q, \tau) = -\frac{8\sqrt{2}\pi}{3} \frac{Q^2(1 - R_m)}{Q^2 + m_\pi^2} (1 - \tau)^{3/2} + \mathcal{O}((1 - \tau)^{5/2}), \quad (\text{A29})$$

$$\begin{aligned} \lim_{\tau \rightarrow -1} w_1(Q_1, Q_2, \tau) &= \frac{16\sqrt{2}\pi}{3m_\mu^2} \frac{(1 - R_{m1})Q_1^3 Q_2^3}{(Q_2^2 + m_\pi^2)(Q_1 - Q_2)^2 (4m_\mu^2 + Q_1 Q_2(1 - R_{m1})(1 - R_{m2}))} \\ &\quad \times [-4m_\mu^2 R_{m2} - (Q_2(1 - R_{m2})(Q_1(1 - R_{m1}) + 2Q_2))] (1 + \tau)^{3/2} \\ &\quad + \mathcal{O}((1 + \tau)^{5/2}), \end{aligned} \quad (\text{A30})$$

$$\begin{aligned} \lim_{\tau \rightarrow -1} w_1(Q, Q, \tau) &= \frac{32\sqrt{2}\pi}{3m_\mu^2} \frac{Q^2 (2m_\mu^4 - 2m_\mu^2 Q^2 - Q^4(1 - R_m))}{(Q^2 + m_\pi^2) (4m_\mu^2 + Q^2(1 - R_m))} \sqrt{1 + \tau} \\ &\quad + \mathcal{O}((1 + \tau)^{3/2}), \end{aligned} \quad (\text{A31})$$

$$\begin{aligned}
\lim_{\tau \rightarrow 1} w_2(Q_1, Q_2, \tau) &= -\frac{16\sqrt{2}\pi}{9m_\mu^2} \frac{Q_1^2 Q_2^2}{((Q_1 + Q_2)^2 + m_\pi^2)(Q_1 + Q_2)^3} \\
&\quad \times [Q_1^3(1 - R_{m1}) + Q_2^3(1 - R_{m2}) \\
&\quad + m_\mu^2(Q_1(3 - R_{m1}) + Q_2(3 - R_{m2}))] (1 - \tau)^{3/2} \\
&\quad + \mathcal{O}((1 - \tau)^{5/2}), \tag{A32}
\end{aligned}$$

$$\begin{aligned}
\lim_{\tau \rightarrow 1} w_2(Q, Q, \tau) &= -\frac{4\sqrt{2}\pi}{9m_\mu^2} \frac{Q^2(m_\mu^2(3 - R_m) + Q^2(1 - R_m))}{4Q^2 + m_\pi^2} (1 - \tau)^{3/2} \\
&\quad + \mathcal{O}((1 - \tau)^{5/2}), \tag{A33}
\end{aligned}$$

$$\begin{aligned}
\lim_{\tau \rightarrow -1} w_2(Q_1, Q_2, \tau) &= \frac{16\sqrt{2}\pi}{9m_\mu^2} \frac{Q_1^2 Q_2^2}{((Q_1 - Q_2)^2 + m_\pi^2)(Q_1 - Q_2)^3} \\
&\quad \times [Q_1^3(1 - R_{m1}) - Q_2^3(1 - R_{m2}) \\
&\quad + m_\mu^2(Q_1(3 - R_{m1}) - Q_2(3 - R_{m2}))] (1 + \tau)^{3/2} \\
&\quad + \mathcal{O}((1 + \tau)^{5/2}), \tag{A34}
\end{aligned}$$

$$\begin{aligned}
\lim_{\tau \rightarrow -1} w_2(Q, Q, \tau) &= \frac{8\sqrt{2}\pi}{3m_\mu^2 m_\pi^2} \frac{Q^2(4m_\mu^4 + m_\mu^2 Q^2(5 - 3R_m) + Q^4(1 - R_m))}{4m_\mu^2 + Q^2} \sqrt{1 + \tau} \\
&\quad + \mathcal{O}((1 + \tau)^{3/2}), \tag{A35}
\end{aligned}$$

where

$$R_m = \sqrt{1 + 4m_\mu^2/Q^2}. \tag{A36}$$

The weight functions $w_{1,2}(Q_1, Q_2, \tau)$ vanish for $\tau \rightarrow \pm 1$. However, for $Q_1 = Q_2 = Q$ and $\tau \rightarrow -1$, when the original four-vectors $(Q_1)_\mu$ and $(Q_2)_\mu$ become more and more antiparallel, the approach to zero is much steeper, even with infinite slope, compare Eqs. (A31) and (A35) to the other equations, see also Fig. 3.

B Form factor models

For illustration, we present in this Appendix briefly the definitions of the two form factor models used in the main text. Much more details and all the derivations can be found in Refs. [52, 21, 11]. We use these form factor models only for illustration, since we are interested in the impact of current and future experimental form factor uncertainties on the pseudoscalar-pole contribution to HLbL in the muon $g - 2$. Those uncertainties have been parametrized by the functions $\delta_{1,P}(Q)$ and $\delta_{2,P}(Q_1, Q_2)$ introduced in Eqs. (26) and (27). Therefore we list in the following only the central values of the model parameters and not their uncertainties, which are related to their extraction from experimental data or by imposing theoretical constraints and assumptions.

We first discuss the pion. The form factor is normalized to the decay width $\Gamma(\pi^0 \rightarrow \gamma\gamma) = 7.63 \text{ eV}$ [4] which is quite well reproduced by the chiral anomaly (constant Wess-Zumino-Witten form factor)

$$\mathcal{F}_{\pi^0\gamma^*\gamma^*}(0,0) = \mathcal{F}_{\pi^0\gamma^*\gamma^*}^{\text{WZW}}(q_1^2, q_2^2) \equiv -\frac{N_c}{12\pi^2 F_\pi}, \quad (\text{B1})$$

if one sets $N_c = 3$ and uses the pion decay constant $F_\pi = 92.4 \text{ MeV}$ obtained from the weak decay of the charged pion.

LMD+V model

The LMD+V model for the pion-photon form factor $\mathcal{F}_{\pi^0\gamma^*\gamma^*}(q_1^2, q_2^2)$ is rooted in the Minimal Hadronic Approximation (MHA) [53] to Green's functions in large- N_c QCD. One starts with an ansatz for the three point function $\langle VVP \rangle$ and thus the form factor $\mathcal{F}_{\pi^0\gamma^*\gamma^*}(q_1^2, q_2^2)$ in the chiral limit with one multiplet of the lightest pseudoscalars (Goldstone bosons) and two multiplets of vector resonances ρ and ρ' : Lowest Meson Dominance (LMD) + V. The functions $\langle VVP \rangle$ and $\mathcal{F}_{\pi^0\gamma^*\gamma^*}(q_1^2, q_2^2)$ fulfill all leading and some subleading QCD short-distance constraints from the operator product expansion (OPE) [55].¹⁰

In particular, in the chiral limit, one obtains from the OPE a condition for the form factor when both momenta are equal and large in the Euclidean [56, 57]

$$\lim_{Q^2 \rightarrow \infty} \mathcal{F}_{\pi^0\gamma^*\gamma^*}(-Q^2, -Q^2) = -\frac{2F_\pi}{3} \left\{ \frac{1}{Q^2} - \frac{8}{9} \frac{\delta^2}{Q^4} + \mathcal{O}\left(\frac{1}{Q^6}\right) \right\}, \quad (\text{B2})$$

where $\mathcal{O}(\alpha_s)$ corrections are neglected and the quantity $\delta^2 = (0.2 \pm 0.02) \text{ GeV}^2$ parametrizes the higher-twist matrix element in the OPE in the chiral limit. It was determined in Ref. [57] using QCD sum rules.

Furthermore, one demands that the form factor reproduces the Brodsky-Lepage (BL) [72] behavior for the single-virtual pion-photon transition form factor

$$\lim_{Q^2 \rightarrow \infty} \mathcal{F}_{\pi^0\gamma^*\gamma^*}(-Q^2, 0) = -\frac{2F_\pi}{Q^2} + \mathcal{O}\left(\frac{1}{Q^4}\right). \quad (\text{B3})$$

The LMD+V form then reads [52, 21, 11]

$$\mathcal{F}_{\pi^0\gamma^*\gamma^*}^{\text{LMD+V}}(q_1^2, q_2^2) = \frac{F_\pi}{3} \frac{q_1^2 q_2^2 (q_1^2 + q_2^2) + h_1 (q_1^2 + q_2^2)^2 + \bar{h}_2 q_1^2 q_2^2 + \bar{h}_5 (q_1^2 + q_2^2) + \bar{h}_7}{(q_1^2 - M_{V_1}^2)(q_1^2 - M_{V_2}^2)(q_2^2 - M_{V_1}^2)(q_2^2 - M_{V_2}^2)}, \quad (\text{B4})$$

where we use for the vector meson masses that appear in Eq. (B4) the values from Refs. [52, 21, 11]

$$M_{V_1} = M_\rho = 775.49 \text{ MeV}, \quad (\text{B5})$$

$$M_{V_2} = M_{\rho'} = 1.465 \text{ GeV}. \quad (\text{B6})$$

¹⁰Recently, the ansatz for $\langle VVP \rangle$ was generalized to two-multiplets of pseudoscalars π, π' and two-multiplets of vector mesons ρ, ρ' in Ref. [102].

On the other hand, the constants h_i, \bar{h}_i are the free parameters of the LMD+V model and have been determined in Refs. [52, 21, 22, 11] by several experimental and theoretical constraints:

$$h_1 = 0 \quad (\text{to reproduce the BL behavior (B3)}), \quad (\text{B7})$$

$$\bar{h}_2 = -4(M_{V_1}^2 + M_{V_2}^2) + (16/9)\delta^2 = -10.63 \text{ GeV}^2 \quad (\text{following Ref. [22]}), \quad (\text{B8})$$

$$\bar{h}_5 = (6.93 \pm 0.26) \text{ GeV}^4 \quad (\text{from a fit to CLEO data [67] in Ref. [52]}), \quad (\text{B9})$$

$$\bar{h}_7 = -\frac{N_c M_{V_1}^4 M_{V_2}^4}{4\pi^2 F_\pi^2} = -14.83 \text{ GeV}^6 \quad (\text{from chiral anomaly}). \quad (\text{B10})$$

The OPE condition when all momenta in $\langle VVP \rangle$ are large and all the currents approach one point, uniquely fixes the first term in the numerator in Eq. (B4). This also shows that the form factor cannot factorize in QCD: $\mathcal{F}_{\pi^0 \gamma^* \gamma^*}(q_1^2, q_2^2) \neq f(q_1^2) \times f(q_2^2)$. Note that the OPE (B2) and BL (B3) conditions cannot be simultaneously satisfied with only one vector meson multiplet (LMD form factor), see Ref. [52].

We note that unless δ^2 would be much different than the estimate given below Eq. (B2), the size and in particular the negative sign of \bar{h}_2 is determined almost completely by the first term in Eq. (B8) involving the masses M_{V_1} and M_{V_2} . This leads to tensions to reproduce the decay rate $\pi^0 \rightarrow e^+ e^-$, see Refs. [21, 80].

For completeness, the result for the single-virtual pion-photon transition form factor is given by

$$\mathcal{F}_{\pi^0 \gamma^* \gamma^*}^{\text{LMD+V}}(-Q^2, 0) = \frac{F_\pi}{3} \frac{1}{M_{V_1}^2 M_{V_2}^2} \frac{h_1 Q^4 - \bar{h}_5 Q^2 + \bar{h}_7}{(Q^2 + M_{V_1}^2)(Q^2 + M_{V_2}^2)}. \quad (\text{B11})$$

VMD model

The well-known VMD model is given by

$$\mathcal{F}_{\pi^0 \gamma^* \gamma^*}^{\text{VMD}}(q_1^2, q_2^2) = -\frac{N_c}{12\pi^2 F_\pi} \frac{M_V^4}{(q_1^2 - M_V^2)(q_2^2 - M_V^2)}. \quad (\text{B12})$$

Here the two free model parameters are F_π (normalization of the form factor) and the vector-meson mass $M_V (= M_\rho)$. Note that the VMD model factorizes $\mathcal{F}_{\pi^0 \gamma^* \gamma^*}^{\text{VMD}}(q_1^2, q_2^2) = f(q_1^2) \times f(q_2^2)$. This might be a too simplifying assumption and also contradicts the OPE in QCD. Furthermore, the VMD model has a wrong short-distance behavior:

$$\mathcal{F}_{\pi^0 \gamma^* \gamma^*}^{\text{VMD}}(-Q^2, -Q^2) \sim \frac{1}{Q^4}, \quad \text{for large } Q^2, \quad (\text{B13})$$

i.e. it falls off too fast compared to the OPE prediction in Eq. (B2).

The single-virtual pion-photon transition form factor is given by

$$\mathcal{F}_{\pi^0 \gamma^* \gamma^*}^{\text{VMD}}(-Q^2, 0) = -\frac{N_c}{12\pi^2 F_\pi} \frac{M_V^2}{Q^2 + M_V^2}. \quad (\text{B14})$$

Comparison of the two form factor models

In order to compare the two form factor models, we introduce the abbreviation

$$\Delta\mathcal{F}(Q_1^2, Q_2^2) = \mathcal{F}_{\pi^0\gamma^*\gamma^*}^{\text{LMD+V}}(-Q_1^2, -Q_2^2) - \mathcal{F}_{\pi^0\gamma^*\gamma^*}^{\text{VMD}}(-Q_1^2, -Q_2^2). \quad (\text{B15})$$

In Fig. 7 we plot the LMD+V form factor normalized to $\mathcal{F}_{\pi^0\gamma^*\gamma^*}(0, 0)$ as a function of Q_1 and Q_2 for the given model parameters in the region $Q_{1,2} \leq 2$ GeV which is the most relevant for the pion-pole contribution to the muon $g-2$. As expected, one sees a damping for large momenta. We also plot the difference between the LMD+V and the VMD form factors, expressed through $\Delta\mathcal{F}(Q_1^2, Q_2^2)$, relative to the LMD+V model. In Table 8 we give, for a selection of values of Q_1 and Q_2 , the values for the normalized form factors for the two models and their comparison.

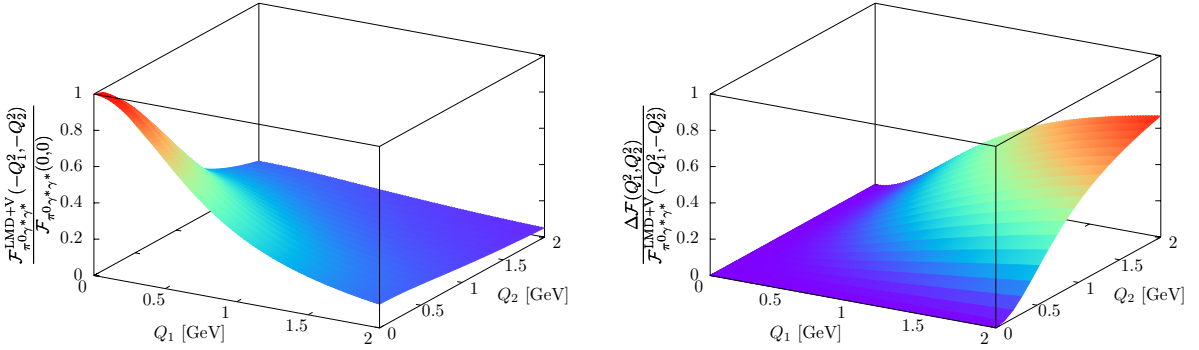


Figure 7: Left panel: normalized LMD+V form factor as a function of Q_1 and Q_2 . Note the linear scale in $Q_{1,2}$. Right panel: relative difference between the LMD+V and VMD form factors.

Note that the form factors in both models reproduce equally well the CLEO data [67] for the single-virtual pion photon transition form factor, once one puts $h_1 = 0$ in the LMD+V model and fits the constant \bar{h}_5 [52]. See Ref. [58] for recent fits to more experimental data. Therefore

$$\mathcal{F}_{\pi^0\gamma^*\gamma^*}^{\text{LMD+V}}(-Q^2, 0) \approx \mathcal{F}_{\pi^0\gamma^*\gamma^*}^{\text{VMD}}(-Q^2, 0). \quad (\text{B16})$$

Since the double-virtual LMD+V and VMD form factors $\mathcal{F}_{\pi^0\gamma^*\gamma^*}(-Q_1^2, -Q_2^2)$ differ for $Q_1 = Q_2 = 1$ [1.5] GeV by 23% [49%], it might be possible to distinguish the two models experimentally at BESIII [42], if the binning is chosen properly, see also Fig. 6 concerning the expected (statistical) measurement precision of the double-virtual form factor. For lower values of $Q_{1,2}$, which are more relevant for the pion-pole contribution to the muon $g-2$, it might not be possible to really distinguish the two models with the currently envisioned data set at BESIII. For instance, for $Q_1 = Q_2 = 0.5$ GeV, the two models differ only by about 3%.

Table 8: Values of the normalized form factors in the LMD+V and VMD models and their absolute and relative difference for some selected momenta.

Q_1 [GeV]	Q_2 [GeV]	$\frac{\mathcal{F}_{\pi^0\gamma^*\gamma^*}^{\text{LMD+V}}(-Q_1^2, -Q_2^2)}{\mathcal{F}_{\pi^0\gamma^*\gamma^*}(0,0)}$	$\frac{\mathcal{F}_{\pi^0\gamma^*\gamma^*}^{\text{VMD}}(-Q_1^2, -Q_2^2)}{\mathcal{F}_{\pi^0\gamma^*\gamma^*}(0,0)}$	$\frac{\Delta\mathcal{F}(Q_1^2, Q_2^2)}{\mathcal{F}_{\pi^0\gamma^*\gamma^*}(0,0)}$	$\frac{\Delta\mathcal{F}(Q_1^2, Q_2^2)}{\mathcal{F}_{\pi^0\gamma^*\gamma^*}^{\text{LMD+V}}(-Q_1^2, -Q_2^2)}$
0.25	0	0.906	0.906	0.00008	0.00009
0.5	0	0.707	0.706	0.0002	0.0003
0.75	0	0.517	0.517	0.0003	0.0006
1	0	0.376	0.376	0.0004	0.001
1.5	0	0.211	0.211	0.0003	0.002
2	0	0.131	0.131	0.0003	0.002
0.25	0.25	0.822	0.821	0.002	0.002
0.5	0.5	0.513	0.499	0.014	0.027
0.75	0.75	0.298	0.267	0.031	0.10
1	1	0.183	0.141	0.042	0.23
1.5	1.5	0.088	0.044	0.043	0.49
2	2	0.052	0.017	0.035	0.67
0.5	0.25	0.645	0.640	0.005	0.007
0.75	0.25	0.475	0.468	0.007	0.015
1	0.25	0.349	0.340	0.008	0.024

Form factors for η and η'

The short-distance analysis in Ref. [52] for the QCD three point function $\langle VVP \rangle$ and the corresponding transition form factor $\mathcal{F}_{P\gamma^*\gamma^*}(q_1^2, q_2^2)$ for the LMD+V ansatz in large- N_c QCD was performed in the chiral limit and assuming octet symmetry. These are certainly not good approximations for the more massive η and η' mesons, where also the nonet symmetry, the effect of the $U(1)_A$ anomaly and the $\eta - \eta'$ -mixing have to be taken into account.

Following Refs. [21, 11], we will therefore use a simple VMD model for η and η' , as for the pion in Eq. (B12), but with the decay constant F_P fixed from the decay width $\Gamma(P \rightarrow \gamma\gamma)$ and the value of M_V obtained from a fit to the CLEO data [67] for the single-virtual transition form factor $\mathcal{F}_{P\gamma^*\gamma^*}(-Q^2, 0)$:

$$\eta - \text{meson:} \quad F_\eta = 93.0 \text{ MeV}, \quad M_V = 774 \text{ MeV}, \quad (\text{B17})$$

$$\eta' - \text{meson:} \quad F_{\eta'} = 74.0 \text{ MeV}, \quad M_V = 859 \text{ MeV}. \quad (\text{B18})$$

References

- [1] F. Jegerlehner, Springer Tracts Mod. Phys. **226**, 1 (2008).
- [2] F. Jegerlehner and A. Nyffeler, Phys. Rept. **477**, 1 (2009).
- [3] J. P. Miller, E. de Rafael, B. L. Roberts and D. Stöckinger, Ann. Rev. Nucl. Part. Sci. **62**, 237 (2012).
- [4] K. A. Olive *et al.* [Particle Data Group Collaboration], Chin. Phys. C **38**, 090001 (2014) and online update 2015.
- [5] G. W. Bennett *et al.*, [Muon g-2 Collaboration], Phys. Rev. D **73**, 072003 (2006).
- [6] P. J. Mohr, B. N. Taylor and D. B. Newell, Rev. Mod. Phys. **80**, 633 (2008).
- [7] T. Aoyama, M. Hayakawa, T. Kinoshita and M. Nio, Phys. Rev. Lett. **109**, 111808 (2012).
- [8] C. Gnendiger, D. Stöckinger and H. Stöckinger-Kim, Phys. Rev. D **88**, 053005 (2013).
- [9] F. Jegerlehner and R. Szafron, Eur. Phys. J. C **71**, 1632 (2011).
- [10] A. Kurz, T. Liu, P. Marquard and M. Steinhauser, Phys. Lett. B **734**, 144 (2014).
- [11] A. Nyffeler, Phys. Rev. D **79**, 073012 (2009).
- [12] G. Colangelo *et al.*, Phys. Lett. B **735**, 90 (2014).
- [13] M. Davier, A. Hoecker, B. Malaescu and Z. Zhang, Eur. Phys. J. C **71**, 1515 (2011) [**72**, 1874(E) (2012)]; M. Davier *et al.*, Eur. Phys. J. C **74**, 2803 (2014); K. Hagiwara *et al.*, J. Phys. G **38**, 085003 (2011); M. Benayoun, P. David, L. DelBuono and F. Jegerlehner, Eur. Phys. J. C **72**, 1848 (2012); Eur. Phys. J. C **73**, 2453 (2013); Eur. Phys. J. C **75**, 613 (2015); talk by T. Teubner at workshop “High-precision QCD at low energy”, 2-22 August 2015, Benasque, Spain; talks by M Benayoun, arXiv:1511.01329 [hep-ph], F. Jegerlehner [14], Z. Zhang, arXiv:1511.05405 [hep-ph] at workshop “Flavour changing and conserving processes (FCCP 2015)”, 10-12 September 2015, Anacapri, Italy.
- [14] F. Jegerlehner, talk at workshop “Flavour changing and conserving processes (FCCP 2015)”, 10-12 September 2015, Anacapri, Italy, arXiv:1511.04473 [hep-ph].
- [15] T. Blum *et al.*, arXiv:1311.2198 [hep-ph]; M. Benayoun *et al.*, arXiv:1407.4021 [hep-ph].
- [16] D. W. Hertzog, talk at workshop “Flavour changing and conserving processes (FCCP 2015)”, 10-12 September 2015, Anacapri, Italy, arXiv:1512.00928 [hep-ex].

- [17] J. Prades, E. de Rafael and A. Vainshtein, Adv. Ser. Direct. High Energy Phys. **20**, 303 (2009) [arXiv:0901.0306 [hep-ph]].
- [18] M. Hayakawa, T. Kinoshita and A. I. Sanda, Phys. Rev. Lett. **75**, 790 (1995); Phys. Rev. D **54**, 3137 (1996).
- [19] M. Hayakawa and T. Kinoshita, Phys. Rev. D **57**, 465 (1998) [**66**, 019902(E) (2002)].
- [20] J. Bijnens, E. Pallante and J. Prades, Phys. Rev. Lett. **75**, 1447 (1995) [**75**, 3781(E) (1995)]; Nucl. Phys. B **474**, 379 (1996); Nucl. Phys. B **626**, 410 (2002).
- [21] M. Knecht and A. Nyffeler, Phys. Rev. D **65**, 073034 (2002).
- [22] K. Melnikov and A. Vainshtein, Phys. Rev. D **70**, 113006 (2004).
- [23] V. Pauk and M. Vanderhaeghen, Eur. Phys. J. C **74**, 3008 (2014).
- [24] F. Jegerlehner, talk at workshop “Hadronic contributions to the muon anomalous magnetic moment”, 1-5 April 2014, Waldthausen Castle, near Mainz, Germany.
- [25] T. Goecke, C. S. Fischer and R. Williams, Phys. Rev. D **83**, 094006 (2011) [**86**, 099901(E) (2012)]; Phys. Rev. D **87**, 034013 (2013).
- [26] A. E. Dorokhov, A. E. Radzhabov and A. S. Zhevlakov, Eur. Phys. J. C **75**, 417 (2015).
- [27] K. T. Engel, H. H. Patel and M. J. Ramsey-Musolf, Phys. Rev. D **86**, 037502 (2012); K. T. Engel, Ph.D. thesis, May 2013; K. T. Engel and M. J. Ramsey-Musolf, Phys. Lett. B **738**, 123 (2014).
- [28] J. Bijnens, talk at workshop “Flavour changing and conserving processes (FCCP 2015)”, 10-12 September 2015, Anacapri, Italy, arXiv:1510.05796 [hep-ph].
- [29] T. Blum *et al.*, Phys. Rev. Lett. **114**, 012001 (2015); T. Blum *et al.*, Phys. Rev. D **93**, 014503 (2016).
- [30] J. Green *et al.*, Phys. Rev. Lett. **115**, 222003 (2015); J. Green *et al.*, arXiv:1510.08384 [hep-lat].
- [31] G. Colangelo, M. Hoferichter, M. Procura and P. Stoffer, JHEP **1409**, 091 (2014); G. Colangelo *et al.*, Phys. Lett. B **738**, 6 (2014); G. Colangelo, M. Hoferichter, M. Procura and P. Stoffer, JHEP **1509**, 074 (2015).
- [32] V. Pauk and M. Vanderhaeghen, arXiv:1403.7503 [hep-ph]; V. Pauk and M. Vanderhaeghen, Phys. Rev. D **90**, 113012 (2014).
- [33] E. Czerwinski *et al.*, arXiv:1207.6556 [hep-ph];
- [34] L. G. Landsberg, Phys. Rept. **128**, 301 (1985).

- [35] F. Jegerlehner, *Acta Phys. Polon. B* **38**, 3021 (2007).
- [36] A. Vainshtein, talk at workshop “Flavour changing and conserving processes (FCCP 2015)”, 10-12 September 2015, Anacapri, Italy.
- [37] In addition to the estimates in Refs. [18, 19, 20, 21, 22, 38, 11, 2, 25, 39, 40], these are: D. K. Hong and D. Kim, *Phys. Lett. B* **680**, 480 (2009); L. Cappiello, O. Cata and G. D’Ambrosio, *Phys. Rev. D* **83**, 093006 (2011); K. Kampf and J. Novotny, *Phys. Rev. D* **84**, 014036 (2011); D. Greynat and E. de Rafael, *JHEP* **1207**, 020 (2012); P. Roig, A. Guevara and G. Lopez Castro, *Phys. Rev. D* **89**, 073016 (2014).
- [38] A. E. Dorokhov and W. Broniowski, *Phys. Rev. D* **78**, 073011 (2008); A. E. Dorokhov, A. E. Radzhabov and A. S. Zhevlakov, *Eur. Phys. J. C* **71**, 1702 (2011); *Eur. Phys. J. C* **72**, 2227 (2012).
- [39] P. Masjuan, *Phys. Rev. D* **86**, 094021 (2012).
- [40] R. Escribano, P. Masjuan and P. Sanchez-Puertas, *Phys. Rev. D* **89**, 034014 (2014).
- [41] G. Eichmann, C. S. Fischer and W. Heupel, *Phys. Rev. D* **92**, 056006 (2015).
- [42] A. Denig, C. Redmer and P. Wasser, private communication.
- [43] K. Johnson, M. Baker and R. Willey, *Phys. Rev.* **136**, B1111 (1964); K. Johnson, R. Willey and M. Baker, *Phys. Rev.* **163**, 1699 (1967); J. L. Rosner, *Annals Phys.* **44**, 11 (1967); M. J. Levine and R. Roskies, *Phys. Rev. D* **9**, 421 (1974); M. J. Levine, E. Remiddi and R. Roskies, *Phys. Rev. D* **20**, 2068 (1979).
- [44] M. Hoferichter *et al.*, *Eur. Phys. J. C* **74**, 3180 (2014).
- [45] C. Hanhart *et al.*, *Eur. Phys. J. C* **73**, 2668 (2013) [**75**, 242(E) (2015)].
- [46] B. Kubis and J. Plenter, *Eur. Phys. J. C* **75**, 283 (2015).
- [47] C. W. Xiao *et al.*, arXiv:1509.02194 [hep-ph].
- [48] J. Wess and B. Zumino, *Phys. Lett. B* **37**, 95 (1971); E. Witten, *Nucl. Phys. B* **223**, 422 (1983).
- [49] In addition to Refs. [21, 25, 23, 26, 28], these are: J. Bijnens and J. Prades, *Mod. Phys. Lett. A* **22**, 767 (2007); M. Z. Abyaneh, arXiv:1208.2554 [hep-ph].
- [50] K. Melnikov, *Int. J. Mod. Phys. A* **16**, 4591 (2001).
- [51] M. Knecht, A. Nyffeler, M. Perrottet and E. de Rafael, *Phys. Rev. Lett.* **88**, 071802 (2002).
- [52] M. Knecht and A. Nyffeler, *Eur. Phys. J. C* **21**, 659 (2001).

- [53] B. Moussallam and J. Stern, hep-ph/9404353; B. Moussallam, Phys. Rev. D **51**, 4939 (1995); Nucl. Phys. B **504**, 381 (1997); S. Peris, M. Perrottet and E. de Rafael, JHEP **9805**, 011 (1998).
- [54] M. Knecht, S. Peris, M. Perrottet and E. de Rafael, Phys. Rev. Lett. **83**, 5230 (1999).
- [55] K. G. Wilson, Phys. Rev. **179**, 1499 (1969); M. A. Shifman, A. I. Vainshtein and V. I. Zakharov, Nucl. Phys. B **147**, 385 (1979); Nucl. Phys. B **147**, 448 (1979).
- [56] V. A. Nesterenko and A. V. Radyushkin, Sov. J. Nucl. Phys. **38**, 284 (1983) [Yad. Fiz. **38**, 476 (1983)].
- [57] V. A. Novikov *et al.*, Nucl. Phys. B **237**, 525 (1984).
- [58] D. Babusci *et al.*, Eur. Phys. J. C **72**, 1917 (2012).
- [59] G. P. Lepage, J. Comput. Phys. **27**, 192 (1978).
- [60] A. Nyffeler, PoS CD **12**, 045 (2013).
- [61] A. M. Bernstein and B. R. Holstein, Rev. Mod. Phys. **85**, 49 (2013).
- [62] K. Kampf, arXiv:1109.4370 [hep-ph].
- [63] I. Larin *et al.* [PrimEx Collaboration], Phys. Rev. Lett. **106**, 162303 (2011).
- [64] A. Gasparian, talk at Chiral Dynamics 2015, June 29 - July 3, 2015, Pisa, Italy.
- [65] J. F. Donoghue, B. R. Holstein and Y. C. R. Lin, Phys. Rev. Lett. **55**, 2766 (1985) [**61**, 1527(E) (1988)]; J. Bijnens, A. Bramon and F. Cornet, Phys. Rev. Lett. **61**, 1453 (1988); B. Ananthanarayan and B. Moussallam, JHEP **0205**, 052 (2002); J. L. Goity, A. M. Bernstein and B. R. Holstein, Phys. Rev. D **66**, 076014 (2002); B. L. Ioffe and A. G. Oganesian, Phys. Lett. B **647**, 389 (2007); K. Kampf and B. Moussallam, Phys. Rev. D **79**, 076005 (2009).
- [66] H. J. Behrend *et al.* [CELLO Collaboration], Z. Phys. C **49**, 401 (1991).
- [67] J. Gronberg *et al.* [CLEO Collaboration], Phys. Rev. D **57**, 33 (1998).
- [68] B. Aubert *et al.* [BaBar Collaboration], Phys. Rev. D **80**, 052002 (2009).
- [69] H. Fonvieille *et al.*, Phys. Lett. B **233**, 65 (1989); R. Meijer Drees *et al.* [SINDRUM-I Collaboration], Phys. Rev. D **45**, 1439 (1992); F. Farzanpay *et al.*, Phys. Lett. B **278**, 413 (1992).
- [70] K. Kampf, M. Knecht and J. Novotny, Eur. Phys. J. C **46**, 191 (2006); T. Husek, K. Kampf and J. Novotny, Phys. Rev. D **92**, 054027 (2015).

- [71] S. Uehara *et al.* [Belle Collaboration], Phys. Rev. D **86**, 092007 (2012);
- [72] G. P. Lepage and S. J. Brodsky, Phys. Lett. B **87**, 359 (1979); Phys. Rev. D **22**, 2157 (1980); S. J. Brodsky and G. P. Lepage, Phys. Rev. D **24**, 1808 (1981).
- [73] A. Nyffeler, PoS CD **09**, 080 (2009).
- [74] A. Denig [BESIII Collaboration], Nucl. Part. Phys. Proc. **260**, 79 (2015).
- [75] M. N. Achasov *et al.* [SND Collaboration], Phys. Lett. B **559**, 171 (2003); R. R. Akhmetshin *et al.* [CMD-2 Collaboration], Phys. Lett. B **605**, 26 (2005).
- [76] M. Hoferichter and B. Kubis, private communication.
- [77] E. Abouzaid *et al.* [KTeV Collaboration], Phys. Rev. Lett. **100**, 182001 (2008).
- [78] A. R. Barker, H. Huang, P. A. Toale and J. Engle, Phys. Rev. D **67**, 033008 (2003).
- [79] E. Abouzaid *et al.* [KTeV Collaboration], Phys. Rev. D **75**, 012004 (2007).
- [80] M. J. Ramsey-Musolf and M. B. Wise, Phys. Rev. Lett. **89**, 041601 (2002); A. E. Dorokhov and M. A. Ivanov, JETP Lett. **87**, 531 (2008); P. Masjuan and P. Sanchez-Puertas, arXiv:1504.07001 [hep-ph].
- [81] P. Vasko and J. Novotny, JHEP **1110**, 122 (2011). T. Husek, K. Kampf and J. Novotny, Eur. Phys. J. C **74**, 3010 (2014).
- [82] S. D. Cohen, H. W. Lin, J. Dudek and R. G. Edwards, PoS (LATTICE 2008), 159 (2008); H. W. Lin and S. D. Cohen, PoS (Confinement X), 113 (2012).
- [83] E. Shintani *et al.* [JLQCD Collaboration], PoS (LAT 2009), 246 (2009); X. Feng *et al.* [JLQCD Collaboration], PoS (Lattice 2011), 154 (2011); X. Feng *et al.* [JLQCD Collaboration], Phys. Rev. Lett. **109**, 182001 (2012).
- [84] H. Czyż and S. Ivashyn, Comput. Phys. Commun. **182**, 1338 (2011); H. Czyż, S. Ivashyn, A. Korchin and O. Shekhovtsova, Phys. Rev. D **85**, 094010 (2012).
- [85] D. Babusci *et al.* [KLOE-2 Collaboration], JHEP **1301**, 119 (2013).
- [86] R. Arnaldi *et al.* [NA60 Collaboration], Phys. Lett. B **677**, 260 (2009).
- [87] G. Usai [NA60 Collaboration], Nucl. Phys. A **855**, 189 (2011).
- [88] P. Aguar-Bartolome *et al.* [A2 Collaboration], Phys. Rev. C **89**, 044608 (2014).
- [89] R. Escribano, P. Masjuan and P. Sanchez-Puertas, Eur. Phys. J. C **75**, 414 (2015).
- [90] H. Aihara *et al.* [TPC/Two Gamma Collaboration], Phys. Rev. Lett. **64**, 172 (1990).
- [91] P. del Amo Sanchez *et al.* [BaBar Collaboration], Phys. Rev. D **84**, 052001 (2011).

- [92] B. Aubert *et al.* [BaBar Collaboration], Phys. Rev. D **74**, 012002 (2006).
- [93] L. Ametller, J. Bijnens, A. Bramon and F. Cornet, Phys. Rev. D **45**, 986 (1992).
- [94] F. Ambrosino *et al.* [KLOE and KLOE-2 Collaborations], Phys. Lett. B **702**, 324 (2011).
- [95] P. Masjuan and P. Sanchez-Puertas, arXiv:1512.09292 [hep-ph].
- [96] M. Acciarri *et al.* [L3 Collaboration], Phys. Lett. B **418**, 399 (1998).
- [97] M. Ablikim *et al.* [BESIII Collaboration], Phys. Rev. D **92**, 012001 (2015).
- [98] R. I. Dzhelyadin *et al.*, Phys. Lett. B **88**, 379 (1979).
- [99] C. Berger *et al.* [PLUTO Collaboration], Phys. Lett. B **142**, 125 (1984).
- [100] R. Escribano, S. Gonzalez-Solis, P. Masjuan and P. Sanchez-Puertas, arXiv:1512.07520 [hep-ph].
- [101] J. Bijnens, talk at workshop “Hadronic contributions to the muon anomalous magnetic moment”, 1-5 April 2014, Waldthausen Castle, near Mainz, Germany.
- [102] T. Husek and S. Leupold, Eur. Phys. J. C **75**, 586 (2015).